applied sciences

MDPI

Article

Extended State Observer-Based Adaptive Neural Networks Backstepping Control for Pneumatic Active Suspension with Prescribed Performance Constraint

Cong Minh Ho and Kyoung Kwan Ahn *

School of Mechanical and Automotive Engineering, University of Ulsan, Ulsan 44610, Republic of Korea
* Correspondence: kkahn@ulsan.ac.kr

Abstract: Pneumatic actuator is one of the key technologies in the field of active suspension due to its low cost, cleanliness, and high power-to-weight ratio characteristics. However, the dynamic models and control strategies of the pneumatic suspension have not been well demonstrated because they are nonlinear systems. Besides, the vertical displacement stability of sprung mass is very important for ensuring ride comfort, but accurate control is still a challenging problem in the presence of parametric uncertainties. In this study, an adaptive neural networks backstepping scheme is designed for the stability control of the pneumatic suspension. Firstly, a mathematical model of the pneumatic system is studied to investigate the dynamic system behavior and to obtain the control algorithm. Secondly, an extended state observer is applied to estimate uncertain parameters, unmodeled dynamics, and external disturbances. Thirdly, unknown masses of various load passengers are approximated by using radial basis function neural networks (RBFNNs). To enhance the system stability, a proposed control with a prescribed performance function (PPF) is designed to guarantee the vertical displacement of the chassis. Adaptive backstepping control with PPF is developed to stabilize the perturbed system and guarantee tracking performance. Finally, the simulation examples for the pneumatic suspension are employed to investigate the effectiveness of the proposed method.

Keywords: pneumatic active suspension; extended state observer (ESO); prescribed performance control (PPC); neural networks; adaptive backstepping

check for updates

Citation: Ho, C.M.; Ahn, K.K. Extended State Observer-Based Adaptive Neural Networks Backstepping Control for Pneumatic Active Suspension with Prescribed Performance Constraint. *Appl. Sci.* **2023**, *13*, 1705. https://doi.org/10.3390/app13031705

Academic Editor: Junhong Park

Received: 16 December 2022
Revised: 30 December 2022
Accepted: 25 January 2023
Published: 29 January 2023

Copyright: © 2023 by the authors. Licensee MDPI, Basel, Switzerland. This article is an open access article distributed under the terms and conditions of the Creative Commons Attribution (CC BY) license (https://creativecommons.org/licenses/by/4.0/).

1. Introduction

The study of suspension systems is an important research area because they isolate the chassis from road disturbances to ensure ride comfort and driving safety for vehicles [1,2]. Compared to passive suspension, an actuator is used for active suspension to provide the active force to dissipate the continuous excitations [3–5]. With the rapid development of technology, various types of actuators such as hydraulic [6], electromagnetic [7], and pneumatic [8] have been used to improve suspension performance. In particular, the pneumatic springs are of more interest as they can supply variable stiffness and damping for different sprung masses by controlling the internal pressure [9]. However, it is difficult either to model or control the pneumatic suspension because of unknown parameters and unmodeled dynamics [10]. Besides, the air bellows become stiffer as the static load increases, so the air spring force is nonlinear in relation to deflection [11], and height adjustment [12]. Due to the difficulty in obtaining the exact parameters of pneumatic servo systems, it is not easy to design a higher-performance tracking controller, especially to maintain chassis stability under various loads of passengers.

To overcome the above drawbacks, many control strategies have been widely used to improve vehicle performance, such as adaptive control [13], optimal control [14], sliding mode control [15], backstepping control [16], and model predictive control [17]. A.J. Nieto et al. [13] developed an adaptive control scheme, which can modify the stiffness coefficient and natural frequency. To obtain the stiffness and ride height of the vehicle

simultaneously, P. Karimi Eskandary et al. [14] discussed the optimized control design by controlling the air pressure. Hyunsup Kim et al. [11] proposed a sliding mode control to improve the tracking accuracy of the chassis stability and overcome nonlinear parameters. Although the robust control can improve the suspension performance, the controller may be sensitive to external disturbances due to the fixed control parameters. Rongchen Zhao et al. [16] proposed backstepping control to solve the problem of height tracking, which is considered the nonlinear model. Xiaoqiang Sun et al. [18] used model predictive control to regulate the vehicle height and adjust both of the roll and pitch angles of the chassis simultaneously. However, due to the unmodeled dynamics of air bellow, it is difficult to establish an accurate linearization model for pneumatic suspension.

In order to improve the control accuracy of nonlinear systems, various disturbance rejection control methods have been widely studied [4,19–21]. Meanwhile, an ESO is useful for solving the effects of unknown parameters, which asymptotically rejects the external disturbance based on the observer bandwidth [22]. ESO considers the external disturbances and the unknown system dynamics as a new state variable, and then the observer gain is proposed to estimate the lumped uncertainties [20]. Therefore, ESO is not only able to approximate parametric uncertainties, but it can also effectively estimate the unknown states of the system [23]. L. Zhao et al. [24] proposed a nonlinear extended state observer-based integral sliding mode control method for a pneumatic servo system with different loads. Besides, ESO is suitable for the unmodeled dynamics of the uncertain system because it is dependent on the system states and requires minimum information about a dynamic system [25]. Due to its high convenience and efficiency, the ESO has been widely used in nonlinear systems such as hydraulic, pneumatic, and robotics control [26,27], and will be applied to estimate the air bellow dynamic in this study.

Over the past decade, with the development of artificial intelligence technology, neural networks and fuzzy logic systems have become powerful tools that can effectively deal with unknown functions or parameters in pneumatic systems [28,29]. NNs have been applied to design robust, adaptive, and intelligent control systems [30,31]. W. N. Bao et al. [32] proposed a fuzzy adaptive sliding mode controller for a pneumatic suspension, which could improve passenger comfort and vehicle controllability. Jing Zhao et al. [33] focused on the ride height adjustment of the pneumatic suspension based on a variable speed fuzzy PWM control method. However, the authors did not consider robust system control in the presence of unknown parameters or unmodeled dynamics. Furthermore, the transient tracking performance cannot be guaranteed quantitatively in all aforementioned control methods [34]. In this study, NNs is employed to approximate unknown nonlinear functions, caused by different sprung masses to ensure the vertical displacement of the chassis.

On the other hand, a new control scheme with output constraints called prescribed performance control was developed by Bechlioulis to ensure the convergence of system outputs, maximum overshoot, and steady-state error into an arbitrarily small predefined region [35–37]. With PPC, a prescribed performance function is defined to transform the tracking error of the original system into a new coordinate. Then, the control scheme will be designed based on a transformed error to preserve the tracking error always within the PPF when the transformed system is stable. PPC has been applied in many control engineering applications that require output constraints [38,39]. Shubo Wang et al. [40] proposed an adaptive funnel control with PPF to guarantee the output error for the servomechanisms system. Jing Na et al. [41] proposed an adaptive control for active suspensions with parametric uncertainties to stabilize the vertical and pitch displacements. Yan-Jun Liu et al. [42] propose an adaptive control with PPF constraint to characterize the tracking error convergence rate and maximum overshoot of the suspension system when actuator failure occurs. However, these results were derived under a full state measurement requirement which is rarely satisfied in practical applications [43] and the external disturbances have a negative impact on the control performance [44]. In this study, the PPF constraint is assigned to guarantee the output performance of a pneumatic suspension with unknown parameters.

According to the above discussions, we first propose a new active suspension system using the air bellow actuator in this paper. Although the pneumatic actuator can fulfill the requirements of a flexible suspension, the stabilization control for the chassis is a challenge since the pneumatic system contains uncertain parameters and external disturbances. Therefore, an ESO is used to estimate these unknown dynamics, where all internal and external disturbances are lumped together and represented by an extended state in this study. Also, the air pressure inside the pneumatic spring is not directly measured by the sensor, so it should be estimated by ESO. Hence, both system states and the extended state could be estimated simultaneously. In real active suspension, the sprung mass is a flexible parameter that can vary due to different passenger masses and will seriously degrade the system performance. Thus, an adaptive NNs backstepping controller is used to overcome the parametric uncertainties. The estimated dynamics are then incorporated with PPF constraint to guarantee the ride height tracking for a pneumatic active suspension system. Moreover, it was found that the unknown parameters may cause the singularity and instability problem of PPC. By using neural networks and ESO, an adaptive backstepping controller is proposed to ensure that the output error remains within prescribed performance constraints. Based on the Lyapunov function stability analysis, all system states and tracking errors can be guaranteed to converge to a small neighborhood of the origin in a finite time and do not violate the constraint boundary. The main contributions of this study can be listed as follows

1. Adaptive backstepping control based PPF is proposed for the pneumatic active suspension to guarantee the stability of sprung mass displacement in the presence of uncertain nonlinear factors.
2. An ESO is issued to estimate the unknown lumped parameters of air bellow, i.e., parametric uncertainties, unmodeled dynamics, and external disturbances.
3. RBFNNs are applied to compensate for the unknown various loads of passengers.

The remainder of this paper is arranged as follows. The nonlinear mathematical of the quarter car model is established in Section 2. Adaptive Neural Network Backstepping Control with PPF and ESO will be proposed while the system stability is improved in Section 3. Besides, the comparative simulations are analyzed in Section 4. Finally, the conclusion of pneumatic active suspension is taken place in Section 5.

2. System Description

2.1. Quarter Car Suspension Model

The quarter suspension model using a pneumatic actuator is displayed in Figure 1. The sprung mass m_{ch} denotes the total weight of the chassis structure and passenger while the unsprung mass m_{us} is composed of the assembly of the vehicle axis and wheel. The stiffness coefficient of the linear spring is defined by k_{sp} while the damping coefficient c_d of the damper is designed as passive components of the suspension system. The tire is modeled by a linear spring with a stiffness coefficient k_{dt} and the damping of the tire is represented by c_{dt}. To create the active force F_a, a pneumatic spring is used for the suspension, which is installed between the chassis and unsprung mass. Besides, the nonlinear stiffness coefficient k_{ap} of air bellow will contribute to the total stiffness of the system. The position of the chassis and unsprung mass will be determined by system state variables z_{ch} and z_{us} while road profile will be presented by z_{rp}.

The dynamic equations of the quarter car model are given as

$$\begin{aligned} m_{ch}\ddot{z}_{ch} &= -F_{sp}(z_{ch}, z_{us}, t) - F_{da}(\dot{z}_{ch}, \dot{z}_{us}, t) + F_a \\ m_{us}\ddot{z}_{us} &= F_{sp}(z_{ch}, z_{us}, t) + F_{da}(\dot{z}_{ch}, \dot{z}_{us}, t) - F_{spt}(z_{us}, z_{rp}t) - F_{dat}(\dot{z}_{us}, \dot{z}_{rp}, t) - F_a \end{aligned} \tag{1}$$

These forces, which are created by the stiffness of pneumatic spring, mechanical springs, and tires, can be expressed as $F_{sp}(z_{ch}, z_{us}, t) = (k_{sp} + k_{ap})(z_{ch} - z_{us})$, $F_{da}(\dot{z}_{ch}, \dot{z}_{us}, t) = c_d(\dot{z}_{ch} - \dot{z}_{us}), F_{spt}(z_{us}, z_{rp}t) = k_{dt}(z_{us} - z_{rd}), F_{dat}(\dot{z}_{us}, \dot{z}_{rp}, t) = c_{dt}(\dot{z}_{us} - \dot{z}_{rd})$.

The expression for the tire force depends on the road holding condition which is given by the following equation [45]

$$F_{tr} = \begin{cases} F_{spt} + F_{dat} & if\ F_{spt} + F_{dat} < (m_{ch} + m_{us})g \\ 0 & if\ F_{spt} + F_{dat} \geq (m_{ch} + m_{us})g \end{cases} \tag{2}$$

where g is the acceleration of gravity.

Define new state variables: $x_1 = z_{ch}$, $x_2 = \dot{z}_{ch}$, $x_3 = z_{us}$, $x_4 = \dot{z}_{us}$, dynamic equations of quarter vehicle suspension can be described by state space as follows

$$\begin{aligned} \dot{x}_1 &= x_2 \\ \dot{x}_2 &= \tfrac{1}{m_{ch}}\left[-F_{sp}(x_1, x_3, t) - F_{da}(x_2, x_4, t) + F_a\right] \\ \dot{x}_3 &= x_4 \\ \dot{x}_4 &= \tfrac{1}{m_{us}}\left[-F_{spt}(x_3, z_{rp}, t) - F_{dat}(x_4, \dot{z}_{rp}, t) + F_{sp}(x_1, x_3, t) + F_{da}(x_2, x_4, t) - F_a\right] \end{aligned} \tag{3}$$

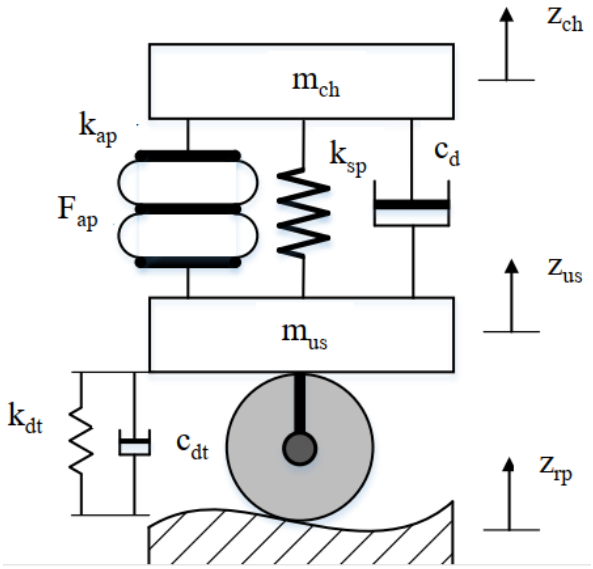

Figure 1. Pneumatic active suspension.

2.2. Air Spring Modeling

An air spring is installed between the chassis and unsprung masses to create the active force which can regulate the displacement for the active suspension system. This external force can be controlled by regulating the supply pressure and is computed by

$$F_a = A_{\text{as}} P_{as} \tag{4}$$

where A_{as} denotes the effective working area and P_{as} is defined as the working pressure inside the pneumatic spring.

Although the pressure inside the air spring is controlled by the airflow, it is also affected by the working conditions, including unmodeled dynamics and parametric uncertainties. Hence, we can describe its nonlinear dynamic model by [11]

$$\dot{P}_{as} = \frac{\kappa RT}{v_{as}}\left(a_0 q_{as} - \frac{P_{as} A_{as}(x_2 - x_4)}{RT}\right) \tag{5}$$

where κ is the polytropic index, R is the ideal air constant, T denotes the gas temperature, v_{as} represents the volume of pneumatic spring, a_0 defines the orifice open area of the solenoid valve, q_{as} and denotes the working area of mass flow rate.

The air bellow volume can be calculated by the initial height and relative movement of the chassis and unsprung mass, we have:

$$v_{as} = A_{as}(z_{as0} + x_1 - x_3) \tag{6}$$

where z_{as0} is the normal height of the pneumatic spring.

Assumption 1. *In this study, it is assumed that the valve spool movement is directly proportional to the voltage parameter applied to the pressure control valve. Thus, the dynamic characteristics of servo valve could be neglected in model construction while the orifice working area a_0 of the control valve is demonstrated by*

$$a_0 = \sigma_{pc} u \tag{7}$$

where σ_{pc} denotes the coefficient control factor and u represents the control voltage.

Substituting (6) and (7) into (5), we can obtain the dynamic model

$$\dot{P}_{as} = \frac{\kappa RT}{A_{as}(z_{as0} + x_1 - x_3)} \left(\sigma_{pc} q_{as} u - \frac{P_{as} A_{as} (x_2 - x_4)}{RT} \right) \tag{8}$$

Consider $x_5 = A_{as} P_{as} / m_{ch}$, the dynamic model of the pneumatic actuator is rewritten

$$\dot{x}_5 = \frac{\kappa RT}{m_{ch}(z_{as0} + x_1 - x_3)} \sigma_{pc} q_{as} u - \frac{\kappa}{(z_{as0} + x_1 - x_3)} x_5 (x_2 - x_4) \tag{9}$$

2.3. Problem Formulation

Different from linear springs, the stiffness coefficient k_{ap} of pneumatic spring is related to the working supply pressure and is affected by many uncertain parameters that are not easy to determine. Although some researchers have studied thermodynamic theory to investigate the response of air bellow under pneumatic suspension [46], applying for the control scheme design is not easy since uncertain working conditions. Since the stiffness coefficient of a pneumatic spring contains uncertain parameters, an unknown continuous function is defined based on a system parameter.

$$d_0 = \frac{1}{m_{ch}} \left[-k_{ap}(x_1 - x_3) \right] \tag{10}$$

In general, the working pressure of a pneumatic spring depends on parametric uncertainties caused by external disturbances, payload variations, and unmodeled dynamics. Therefore the dynamic equation of air spring (9) should be considered unknown parameters defined in the unmodeled terms. Moreover, the inside pressure of the air spring P_{as} is not directly measured by the sensors, so it must be estimated by using an ESO.

Applying the stiffness coefficient, external disturbance, and uncertain parameters of pneumatic spring, the dynamic model of the quarter car suspension can be fully described by (11)

$$\begin{aligned}
\dot{x}_1 &= x_2 \\
\dot{x}_2 &= x_5 + \tfrac{1}{m_{ch}} \left[-k_{sp}(x_1 - x_3) - c_d(x_2 - x_4) \right] + d_0 + d(t) \\
\dot{x}_3 &= x_4 \\
\dot{x}_4 &= \tfrac{1}{m_{us}} \left[-k_{dt}(x_3 - z_{rp}) - c_{dt}(x_4 - \dot{z}_{rp}) + k_{sp}(x_1 - x_3) + c_d(x_2 - x_4) - m_{ch} x_5 - m_{ch} d_0 \right] \\
\dot{x}_5 &= \tfrac{\kappa RT}{m_{ch}(z_{as0} + x_1 - x_3)} \sigma_{pc} q_{as} u - \tfrac{\kappa}{(z_{as0} + x_1 - x_3)} x_5 (x_2 - x_4) \; + p_0 + p(t)
\end{aligned} \tag{11}$$

where $d(t)$ are the lumped modeling errors of sprung mass velocity, p_0 is constant modeling error which affects the accuracy of the pressure measurement equipment, and $p_0(t)$ is time-varying pressure error of pneumatic spring, including parametric uncertainties of unmodeled dynamics and external disturbances.

Assumption 2. *Due to the mechanical structure of vehicle suspension depending on physical performance, the total weight of the sprung mass is bounded by* $m_{\text{smin}} < m_s < m_{\text{smax}}$.

Assumption 3. $d(t)$ *is the unknown bounded time-varying disturbance and satisfies* $|d(t)| \leq |d(t)|_{\max}$.

In this study, a novel controller is developed to satisfy three performance requirements of the vehicle suspension system

(1) Passenger comfort: Adaptive backstepping control is designed to stabilize the chassis and dissipate the external continuous excitations that improve the comfort for passengers.

(2) Road holding: The tire is always kept in contact with the road surface by remaining the relative tire fore (*RTF*) should not exceed one. *RTF* is used to evaluate the driving safety factor which is defined by comparing the dynamic tire force with the total weight of the chassis structure, wheel, and tire

$$RTF = \frac{F_t}{(m_s + m_u)g} \tag{12}$$

(3) Suspension deflection: This objective guarantees that the suspension displacement is always limited within the mechanical structure. For this purpose, relative suspension deflection (*RSD*) is used as the constraint value to specify the maximum value of chassis stroke

$$RSD = \frac{z_s - z_u}{z_R} \tag{13}$$

where z_R is determined by the initial distance of the chassis at a rest position which is called rattle space.

Remark 1. *To improve the ride passenger comfort, many advanced control schemes have been applied to dissipate the chassis vibration. Nonetheless, the objectives of improving passenger comfort and ensuring the suspension deflection will conflict with each other. In this study, the chassis movement will be converged to zero by PPF constraint, and the handling stability is satisfied simultaneously. Besides, the ESO and NNs are combined to estimate and compensate for the effects of uncertain parameters so that the tracking errors do not violate the prescribed constraints.*

3. Adaptive Neural Network Backstepping Control with Prescribed Performance and Extended State Observer

In this section, the displacement of sprung mass under road disturbance will be guaranteed within boundary constraints to satisfy the control performance of the active suspension by the proposed control scheme. For this purpose, consider the state space of the chassis dynamic equations by

$$\begin{aligned} \dot{x}_1 &= x_2 \\ \dot{x}_2 &= x_5 + \tfrac{1}{m_{ch}}\left[-k_{sp}(x_1 - x_3) - c_d(x_2 - x_4)\right] + d_0 + d(t) \\ \dot{x}_5 &= \tfrac{\kappa RT}{m_{ch}(z_{as0} + x_1 - x_3)}\sigma_{pc} q_{as} u - \tfrac{\kappa}{(z_{as0} + x_1 - x_3)} x_5(x_2 - x_4) + p_0 + p(t) \end{aligned} \tag{14}$$

Four main objectives of the proposed controller

1. An ESO control scheme can estimate uncertain parameters and unmodeled dynamics.
2. The chassis displacement is limited to specific PPF constraints.
3. Ensure the suspension performance by considering road holding and keeping the minimum of suspension deflection.
4. The control scheme is proposed by using adaptive NNs combined with ESO and the prescribed performance constraint. Two control approaches are analyzed to compare the effectiveness of the developed control, which are traditional backstepping and ESO backstepping.

3.1. Prescribed Performance Constraint

In this section, a PPC theory is applied for the control scheme to ensure the stability of the chassis in vertical displacement. First, the tracking error of the system state x_1 is defined by

$$e_1 = x_1 - x_d \tag{15}$$

where x_d is the reference trajectory.

Definition 1. *A positive decreasing smooth function is used as the prescribed performance function* [35]:

$$\rho(t) = (\rho_0 - \rho_\infty)e^{-\varphi t} + \rho_\infty \tag{16}$$

where $\varphi > 0$ represents the convergence rate, ρ_0 denotes the initial state of PPF, and ρ_∞ is the allowable steady-state error, which are selected to meet the initial conditions $\lim_{t\to 0}\rho(t) = \rho_0 > 0$, $\lim_{t\to\infty}\rho(t) = \rho_\infty > 0$, and $\rho_0 > \rho_\infty$.

According to (16), the tracking error of chassis movement will be ensured within the bounded performance by the transform inequality

$$-\underline{\kappa}\rho(t) < e_1 < \overline{\kappa}\rho(t),\ t > 0 \tag{17}$$

where $\underline{\kappa}, \overline{\kappa} > 0$ are the constant parameters.

Remark 2. *From (16) and (17), it can be seen that $-\underline{\kappa}\rho(0)$ plays a role as the lower bound of the undershoot while $\overline{\kappa}\rho(0)$ representing the upper bound of the overshoot of x_1. The steady-state performance of the system can be guaranteed by accordingly choosing the design parameters $\underline{\kappa}$, $\overline{\kappa}$, ρ_0, ρ_∞, φ.*

Under the condition (17), the control strategy is designed by using an output transformation, which is used to construct the constraints into an equality form. By suggesting a smooth and strictly increasing function $S(z_1)$, we can obtain [35]

$$S(z_1) = \frac{\overline{\kappa}e^{z_1} - \underline{\kappa}e^{-z_1}}{e^{z_1} + e^{-z_1}} \tag{18}$$

where the two following conditions are satisfied

(1) $-\underline{\kappa} < S(z_1) < \overline{\kappa}$
(2) $\lim_{z_1\to\infty} S(z_1) = \overline{\kappa}$, $\lim_{z_1\to-\infty} S(z_1) = -\underline{\kappa}$

Therefore, we can write the performance (17) as follows

$$e_1 = \rho(t)S(z_1) \tag{19}$$

From the above definition, prescribed performance can be designed to establish the transform errors of system states. Since $S(z_1)$ is strictly monotonically increasing and prescribed performance parameters are selected to satisfy $\rho(t) > \rho_\infty > 0$, we can conclude an inverse transfer function z_1 as follows

$$z_1 = S^{-1}\left(\frac{e_1}{\rho(t)}\right) \tag{20}$$

So, we have the transform function of z_1

$$z_1 = \frac{1}{2}\ln\left(\frac{\mu + \underline{\kappa}}{\overline{\kappa} - \mu}\right), \tag{21}$$

where $\mu = \frac{e_1}{\rho(t)}$.

Lemma 1. [35]. *From the above procedure, the system state (14) is transformed by the smooth function $S(z_1)$, so the tracking error signal e_1 is guaranteed under the prescribed performance boundary (17).*

Remark 3. *Based on the above analysis, as the parameters $\rho_0, \underline{\kappa}, \overline{\kappa}$ are designed such that the initial condition satisfies $-\underline{\kappa}\rho(0) < x_1(0) < \overline{\kappa}\rho(0)$ and z_1 will be restrained within the boundaries, the condition $-\underline{\kappa} < S(z_1) < \overline{\kappa}$ is guaranteed. Therefore, the control problem (14) with the condition $-\underline{\kappa}\rho(t) < x_1(t) < \overline{\kappa}\rho(t)$ is ensured by the transformation (20).*

3.2. Extended State Observer

As mentioned in Section 2, there always exist uncertain parameters, external disturbances, and unmodeled dynamics in the nonlinear pneumatic system, which will degrade the performance of the suspension controller. ESO is used to compensate for these unknown terms in this study. Firstly, all lumped uncertainties are considered as broadening unknown system states. Secondly, an ESO is proposed to estimate these system states by designing parameter estimators and suggesting the control law to approximate unmodeled dynamics. Thus, ESO can not only compensate for unknown parameters but also enhance the robustness of the vehicle suspension [47].

To design an ESO, an additional state variable x_6 is proposed to express the lumped unknown dynamics $p_0 + p(t)$ as follows

$$x_6 = p_0 + p(t) \tag{22}$$

Then, the system variables are expanded to $x = [x_1, x_2, x_5, x_6]^T$. So, the original system (14) can be extended by

$$\begin{aligned} \dot{x}_1 &= x_2 \\ \dot{x}_2 &= x_5 + f_1(x_1, x_2) + d_0 + d(t) \\ \dot{x}_5 &= f_2(x_1, x_2, x_5) + g(x_1)u + x_6 \\ \dot{x}_6 &= h(t) \end{aligned} \tag{23}$$

where $f_1(x_1, x_2) = (1/m_{ch})[-k_{sp}(x_1 - x_3) - c_d(x_2 - x_4)]$, $f_2(x_1, x_2, x_5) = [-\kappa/(z_{as0} + x_1 - x_3)]x_5(x_2 - x_4)$, $g(x_1) = \{\kappa RT/[m_{ch}(z_{as0} + x_1 - x_3)]\}\sigma_{pc}q_{as}$, and $h(t)$ denotes the time derivative of x_6.

From (23), the ESO design can not only observe incorrectly measured system variables x_2, x_5 but also estimate the model uncertainty x_6 to compensate the controller in real-time.

Assumption 4. *To simplify the ESO design, the lumped dynamicx_6 is adopted with a limited derivative, i.e., $h(t)$ is bounded.*

Assumption 5. *The functions $f_1(x_1, x_2)$,$f_2(x_1, x_2, x_5)$, and $g(x_1)$ are considered Lipschitz functions with their state variables.*

According to [48], a linear ESO model is demonstrated for the extended system variables (23) as

$$\begin{aligned} \dot{\hat{x}}_1 &= \hat{x}_2 + 4\omega_0(x_1 - \hat{x}_1) \\ \dot{\hat{x}}_2 &= \hat{x}_5 + f_1(\hat{x}_1, \hat{x}_2) + 6\omega_0^2(x_1 - \hat{x}_1) \\ \dot{\hat{x}}_5 &= \hat{x}_6 + f_2(\hat{x}_1, \hat{x}_2, \hat{x}_5) + g(\hat{x}_1)u + 4\omega_0^3(x_1 - \hat{x}_1) \\ \dot{\hat{x}}_6 &= \omega_0^4(x_1 - \hat{x}_1) \end{aligned} \tag{24}$$

where $\hat{x} = [\hat{x}_1, \hat{x}_2, \hat{x}_5, \hat{x}_6]^T$ is the observer states, ω_0 is the tuning parameter of the observer, and represents the bandwidth of the ESO.

The state observer errors are determined by $\widetilde{x}_i = x_i - \hat{x}_i$, $i = 1, 2, 5, 6$. From the system model (23) and ESO (24), the dynamic equations of state observer errors are expressed as

$$\begin{aligned}
\dot{\widetilde{x}}_1 &= \widetilde{x}_2 - 4\omega_0\widetilde{x}_1 \\
\dot{\widetilde{x}}_2 &= \widetilde{x}_5 + [f_1(x_1, x_2) - f_1(\hat{x}_1, \hat{x}_2)] - 6\omega_0^2\widetilde{x}_1 + d_0 + d(t) \\
\dot{\widetilde{x}}_5 &= \widetilde{x}_6 + [f_2(x_1, x_2, x_5) - f_2(\hat{x}_1, \hat{x}_2, \hat{x}_5)] + [g(x_1) - g(\hat{x}_1)]u - 4\omega_0^3\widetilde{x}_1 \\
\dot{\widetilde{x}}_6 &= -\omega_0^4\widetilde{x}_1 + h(t)
\end{aligned} \tag{25}$$

To investigate the convergence of the adopted ESO (24), the scaled estimation errors will be determined by $\varepsilon_i = \widetilde{x}_i/\omega_i^{i-1}$, $i = 1, 2$ and $\varepsilon_j = \widetilde{x}_j/\omega_j^{i-3}$, $j = 5, 6$. Thus, we can write (25) in a compact form (26).

$$\dot{\varepsilon} = \omega_0 A\varepsilon + M\frac{\widetilde{f}_1 + d_0 + d(t)}{\omega_0} + N\frac{\widetilde{f}_2 + \widetilde{g}u}{\omega_0^2} + K\frac{h(t)}{\omega_0^3} \tag{26}$$

where A is a Hurwitz matrix, so there exists a positive definite matrix satisfying $A^TP + PA = -I$

$$A = \begin{bmatrix} -4 & 1 & 0 & 0 \\ -6 & 0 & 1 & 0 \\ -4 & 0 & 0 & 1 \\ -1 & 0 & 0 & 0 \end{bmatrix},\ M = \begin{bmatrix} 0 \\ 1 \\ 0 \\ 0 \end{bmatrix},\ N = \begin{bmatrix} 0 \\ 0 \\ 1 \\ 0 \end{bmatrix},\ K = \begin{bmatrix} 0 \\ 0 \\ 0 \\ 1 \end{bmatrix}$$

$$\varepsilon = [\varepsilon_1, \varepsilon_2, \varepsilon_5, \varepsilon_6]^T; \widetilde{f}_1 = f_1(x_1, x_2) - f_1(\hat{x}_1, \hat{x}_2)$$
$$\widetilde{f}_2 = f_2(x_1, x_2, x_5) - f_2(\hat{x}_1, \hat{x}_2, \hat{x}_5);\ \widetilde{g} = g(x_1) - g(\hat{x}_1)$$

Lemma 2. [49]. *Based on Assumption 4, the state variable $h(t)$ is bounded, so the observer state $\hat{x}_i$ is bounded. Thus, there exist positive constants $\ell_i > 0$ that $|\widetilde{x}_i| < \ell_i$ are satisfied.*

According to Assumption 5, there exist a set of constant values that satisfy the Lipschitz conditions

$$\begin{aligned}
&\widetilde{f}_1 = |f_1(x_1, x_2) - f_1(\hat{x}_1, \hat{x}_2)| \le c_1|\varepsilon_1| + c_2|\varepsilon_2| \le (c_1 + c_2)\|\varepsilon\| \\
&\widetilde{f}_2 = f_2(x_1, x_2, x_5) - f_2(\hat{x}_1, \hat{x}_2, \hat{x}_5) \le c_3|\varepsilon_1| + c_4|\varepsilon_2| + c_5|\varepsilon_5| \ \le (c_3 + c_4 + c_5)\|\varepsilon\| \\
&\widetilde{g} = g(x_1) - g(\hat{x}_1) \le c_6\|\varepsilon\|
\end{aligned} \tag{27}$$

where $\|\varepsilon\| = \sqrt{|\varepsilon_1|^2 + |\varepsilon_2|^2 + |\varepsilon_5|^2 + |\varepsilon_6|^2}$.

Remark 4. *Based on scaled estimation errors (26) and the analysis in Lemma 2, the proposed ESO is stable and the state observer errors are set promptly small by regulating the bandwidth parameter ω_0. It should be set the bandwidth to satisfy the balance between the observer performance and system robustness because a large ω_0 can cause high frequency oscillation of the system. Then, the estimation states $\hat{x}_2$, $\hat{x}_5$, $\hat{x}_6$ in the Equation (24) are used to design the controller.*

3.3. Backstepping Controller Design with PPF and ESO

This section proposes an adaptive control scheme based on a modified backstepping technique, where parametric uncertainties are compensated by the ESO and the PPF is applied to guarantee the tracking error of chassis displacement x_1 in the predefined boundary. Consequently, the Lyapunov Barrier theory is applied to prove the stability of the proposed algorithm scheme.

Step 1: Define the tracking error with PPF in Section 3.1

Step 2: Choose the virtual signal α_1

From (21), the derivative of z_1 can be rewritten as

$$\dot{z}_1 = \frac{1}{2}\left(\frac{1}{\mu + \underline{\kappa}} - \frac{1}{\mu - \overline{\kappa}}\right)\left(\frac{\dot{x}_1}{\rho} - \frac{x_1\dot{\rho}}{\rho^2}\right) = \varsigma\left(x_2 - \frac{x_1\dot{\rho}}{\rho}\right) \tag{28}$$

where $\varsigma = \frac{1}{2\rho}\left(\frac{1}{\mu+\underline{\kappa}} - \frac{1}{\mu-\overline{\kappa}}\right)$.

The error variable of x_2 is defined by

$$z_2 = x_2 - \alpha_1 \tag{29}$$

Choose the candidate Lyapunov function V_1

$$V_1 = \frac{1}{2}z_1^2 \tag{30}$$

The time derivative of V_1 is

$$\dot{V}_1 = z_1\dot{z}_1 \tag{31}$$

Substituting (28) and (29) into (31), we have

$$\dot{V}_1 = z_1\varsigma\left(z_2 + \alpha_1 - \frac{x_1\dot{\rho}}{\rho}\right) \tag{32}$$

Choose the virtual control α_1 as follows

$$\alpha_1 = \frac{x_1\dot{\rho}}{\rho} - \varsigma^{-1}k_1z_1 \tag{33}$$

Substituting (33) into (32), we have the form of $\dot{V}_1$

$$\dot{V}_1 = -k_1z_1^2 + z_1\varsigma z_2 \tag{34}$$

Step 3: Develop the virtual control α_2
Define the error variable of x_5

$$z_3 = x_5 - \alpha_2 \tag{35}$$

Choose the candidate Lyapunov function V_2

$$V_2 = V_1 + \frac{1}{2}z_2^2 \tag{36}$$

The time derivative of V_2 is defined by

$$\dot{V}_2 = \dot{V}_1 + z_2\dot{z}_2 \tag{37}$$

Substituting (29) and (34) into (37), we have

$$\dot{V}_2 = -k_1z_1^2 + z_2\left(z_1\varsigma + \dot{x}_2 - \dot{\alpha}_1\right) \tag{38}$$

According to (23) and (35), we can write (38) as follows

$$\dot{V}_2 = -k_1z_1^2 + z_2\left[z_1\varsigma + (z_3 + \alpha_2) + f_1 + d_0 + d(t) - \dot{\alpha}_1\right] \tag{39}$$

Choose the virtual control α_2 by using the state estimation of ESO, we obtain

$$\alpha_2 = \alpha_{2c} + \alpha_{2u} \tag{40}$$

where $\alpha_{2c} = -z_1\varsigma + \dot{\alpha}_1 - \hat{f}_1$ and $\alpha_{2u} = -k_2(\hat{x}_2 - \alpha_1)$.

The derivative of virtual control α_2 is calculated by

$$\dot{\alpha}_{2c} = \frac{\partial \alpha_2}{\partial t} + \frac{\partial \alpha_2}{\partial x_1}\hat{x}_2 + \frac{\partial \alpha_2}{\partial \hat{x}_2}\dot{\hat{x}}_2 \text{ and } \dot{\alpha}_{2u} = \frac{\partial \alpha_2}{\partial x_1}\widetilde{x}_2 \tag{41}$$

Then, substituting (40) into (39) and using (26), we have

$$\dot{V}_2 = -k_1 z_1^2 + z_2 z_3 + z_2\widetilde{f}_1 - k_2 z_2^2 + k_2 z_2 \omega_0 \varepsilon_1 + z_2(d_0 + d(t)) \tag{42}$$

Step 4: Design the actual control u

Choose the candidate Lyapunov function V_3

$$V_3 = V_2 + \frac{1}{2}z_3^2 \tag{43}$$

The time derivative of V_3 using (35) and (42) can be described by

$$V_3 = -k_1 z_1^2 + z_2\widetilde{f}_1 - k_2 z_2^2 + k_2 z_2 \omega_0 \varepsilon_1 + z_2(d_0 + d(t)) + z_3\left(z_2 + \dot{x}_5 - \dot{\alpha}_2\right) \tag{44}$$

Using (23), we can write (44) as follows

$$V_3 = -k_1 z_1^2 + z_2\widetilde{f}_1 - k_2 z_2^2 + k_2 z_2 \omega_0 \varepsilon_1 + z_2(d_0 + d(t)) + z_3\left(z_2 + g(x_1)u + f_2 + x_6 - \dot{\alpha}_2\right) \tag{45}$$

Propose the actual control u

$$u = g(\hat{x}_1)^{-1}\left[-\hat{f}_2 - (\hat{x}_2 - \alpha_1) - \hat{x}_6 + \dot{\alpha}_{2c} - k_3(\hat{x}_5 - \alpha_2)\right] \tag{46}$$

Substituting (46) into (45), we have:

$$\begin{aligned} V_3 = -k_1 z_1^2 + z_2\widetilde{f}_1 - k_2 z_2^2 + k_2 z_2 \omega_0 \varepsilon_1 + z_2(d_0 + d(t)) + z_3\widetilde{f}_2 + z_3\omega_0^3\varepsilon_6 \\ + z_3(k_1k_2 + 1)\omega_0\varepsilon_2 - k_3 z_3^2 + k_3 z_3 \omega_0^2 \varepsilon_5 \end{aligned} \tag{47}$$

Theorem 1. *Considering the pneumatic active suspension (14) under Assumptions 1–3, the controller (46) and ESO (24) are designed in this study. Then, the proposed control is proposed, in which the tracking errors and scaled state estimation errors ε_i are bounded at the same time, and the tracking error e_1 converges to the boundary of the PPF constraints by selecting the appropriate control parameters.*

Proof. Using ESO estimation, the candidate Lyapunov function V_4 is selected by

$$V_4 = V_3 + \frac{1}{2}\varepsilon^T P \varepsilon \tag{48}$$

Using (47), we can write the time derivative of V_4 as follows

$$\begin{aligned} \dot{V}_4 = -k_1 z_1^2 + z_2\widetilde{f}_1 - k_2 z_2^2 + k_2 z_2 \omega_0 \varepsilon_1 + z_2(d_0 + d(t)) + z_3\widetilde{f}_2 \\ + z_3\omega_0^3\varepsilon_6 + z_3(k_1k_2 + 1)\omega_0\varepsilon_2 - k_3 z_3^2 + k_3 z_3 \omega_0^2 \varepsilon_5 + \tfrac{1}{2}\dot{\varepsilon}^T P\varepsilon + \tfrac{1}{2}\varepsilon^T P\dot{\varepsilon} \end{aligned} \tag{49}$$

Substituting (26) into (49), we have:

$$\begin{aligned} \dot{V}_4 = -k_1 z_1^2 + z_2\widetilde{f}_1 - k_2 z_2^2 + k_2\omega_0\varepsilon_1 z_2 + z_2(d_0 + d(t)) + \widetilde{f}_2 z_3 + \omega_0^3\varepsilon_6 z_3 \\ + (k_1k_2 + 1)\omega_0\varepsilon_2 z_3 - k_3 z_3^2 + k_3\omega_0^2\varepsilon_5 z_3 - \omega_0\|\varepsilon\|^2 + \varepsilon^T PM\tfrac{\widetilde{f}_1}{\omega_0} \\ + \varepsilon^T PN\tfrac{\widetilde{f}_2}{\omega_0^2} + \varepsilon^T PN\tfrac{\widetilde{g}u}{\omega_0^2} + \varepsilon^T PM\tfrac{d_0 + d(t)}{\omega_0} + \varepsilon^T PK\tfrac{h(t)}{\omega_0^3} \end{aligned} \tag{50}$$

Based on the analysis in (27), assuming that the control signal u is bounded, the observer bandwidth ω_0 is proposed to satisfy the upper bound of lumped unknown dynamics, we have

$$\begin{aligned} -\omega_0\|\varepsilon\|^2 + \varepsilon^T PM\tfrac{\widetilde{f}_1}{\omega_0} + \varepsilon^T PN\tfrac{\widetilde{f}_2}{\omega_0^2} + \varepsilon^T PN\tfrac{\widetilde{g}u}{\omega_0^2} \\ \leq \left(-\omega_0 + \tfrac{\phi_1(c_1+c_2)}{\omega_0} + \tfrac{\phi_2(c_3+c_4+c_5)}{\omega_0^2} + \tfrac{\phi_2 c_6}{\omega_0^2}|u|_{\max}\right)\|\varepsilon\|^2 \end{aligned} \tag{51}$$

where $\phi_1 = PM$ and $\phi_2 = PN$.

Since the unknown parameter d_0, the lumped modeling errors $d(t)$, and the parametric uncertainty $h(t)$ are bounded, the upper-bounded of these states can be obtained as follows

$$\begin{aligned} &z_2(d_0 + d(t)) \leq \tfrac{1}{2}z_2^2 + \tfrac{1}{2}(|d_0|_{\max} + |d(t)|_{\max})^2 \\ &\varepsilon^T PM\tfrac{d_0+d(t)}{\omega_0} \leq \tfrac{1}{2}\|\varepsilon\|^2 + \tfrac{\phi_2^2}{2\omega_0^2}(|d_0|_{\max} + |d(t)|_{\max})^2 \\ &\varepsilon^T PK\tfrac{h(t)}{\omega_0^3} \leq \tfrac{1}{2}\|\varepsilon\|^2 + \tfrac{\phi_3^2}{2\omega_0^6}|h(t)|_{\max}^2 \end{aligned} \tag{52}$$

where $\phi_3 = PK$.

Thus, (52) can be further rewritten as follows

$$\begin{aligned} \dot{V}_4 \leq &-k_1 z_1^2 - \left(k_2 - \tfrac{1}{2}\right)z_2^2 - k_3 z_3^2 + (c_1|\varepsilon_1| + c_2|\varepsilon_2|)z_2 + k_2\omega_0\varepsilon_1 z_2 \\ &+\tfrac{1}{2}z_2^2 + \tfrac{1}{2}(|d_0|_{\max} + |d(t)|_{\max})^2 + \|\varepsilon\|^2 + (c_3|\varepsilon_1| + c_4|\varepsilon_2| + c_5|\varepsilon_5|)z_3 \\ &+\omega_0^3\varepsilon_6 z_3 + (k_1k_2+1)\omega_0\varepsilon_2 z_3 + k_3\omega_0^2\varepsilon_5 z_3 + \tfrac{\phi_2^2}{2\omega_0^2}(|d_0|_{\max} + |d(t)|_{\max})^2 \\ &+\tfrac{\phi_3^2}{2\omega_0^6}|h(t)|_{\max}^2 + \left(-\omega_0 + \tfrac{\phi_1(c_1+c_2)}{\omega_0} + \tfrac{\phi_2(c_3+c_4+c_5)}{\omega_0^2} + \tfrac{\phi_2 c_6}{\omega_0^2}|u|_{\max}\right)\|\varepsilon\|^2 \end{aligned} \tag{53}$$

We can set the total upper-bounded of these states as follow

$$\Upsilon = \left(\frac{1}{2} + \frac{\phi_2^2}{2\omega_0^2}\right)(|d_0|_{\max} + |d(t)|_{\max})^2 + \frac{\phi_3^2}{2\omega_0^6}|h(t)|_{\max}^2$$

$$\Xi = \omega_0 - \frac{\phi_1(c_1+c_2)}{\omega_0} - \frac{\phi_2(c_3+c_4+c_5)}{\omega_0^2} - \frac{\phi_2 c_6}{\omega_0^2}|u|_{\max} - 1$$

So, we have

$$\begin{aligned} \dot{V}_4 \leq &-k_1 z_1^2 - \left(k_2 - \tfrac{1}{2}\right)z_2^2 - k_3 z_3^2 - \Xi\|\varepsilon\|^2 + (c_1|\varepsilon_1| + c_2|\varepsilon_2|)z_2 + k_2\omega_0\varepsilon_1 z_2 \\ &+(c_3|\varepsilon_1| + c_4|\varepsilon_2| + c_5|\varepsilon_5|)z_3 + \omega_0^3\varepsilon_6 z_3 + (k_1k_2+1)\omega_0\varepsilon_2 z_3 + k_3\omega_0^2\varepsilon_5 z_3 + \Upsilon \end{aligned} \tag{54}$$

Arrange (54), we get

$$\begin{aligned} \dot{V}_4 \leq &-k_1 z_1^2 - \left(k_2 - \tfrac{1}{2}\right)z_2^2 - k_3 z_3^2 - \Xi\|\varepsilon\|^2 + (c_1 + k_2\omega_0)|\varepsilon_1||z_2| + c_2|\varepsilon_2||z_2| + c_3|\varepsilon_1|z_3 \\ &+\omega_0^3|\varepsilon_6||z_3| + (k_1k_2 + c_4 + 1)\omega_0|\varepsilon_2||z_3| + \left(c_5 + k_3\omega_0^2\right)|\varepsilon_5||z_3| + \Upsilon \end{aligned} \tag{55}$$

Set $\varpi_1 = c_1 + k_2\omega_0$; $\varpi_2 = c_2$; $\varpi_3 = c_3$, $\varpi_4 = (k_1k_2 + c_4 + 1)\omega_0$; $\varpi_5 = c_5 + k_3\omega_0^2$; $\varpi_6 = \omega_0^3$, the inequality (55) can be obtained by

$$\begin{aligned} \dot{V}_4 \leq &-k_1 z_1^2 - \left(k_2 - \tfrac{1}{2}\right)z_2^2 - k_3 z_3^2 + \varpi_1|\varepsilon_1||z_2| + \varpi_2|\varepsilon_2||z_2| - \Xi\|\varepsilon\|^2 + \varpi_3|\varepsilon_1|z_3 \\ &+\varpi_4|\varepsilon_2||z_3| + \varpi_5|\varepsilon_5||z_3| + \varpi_6|\varepsilon_6||z_3| + \Upsilon \end{aligned} \tag{56}$$

Define tracking error states and matrix Γ as follows

$$\Gamma = \begin{bmatrix} k_1 & 0 & 0 & 0 & 0 & 0 & 0 \\ 0 & k_2 - 1/2 & 0 & -\omega_1/2 & -\omega_2/2 & 0 & 0 \\ 0 & 0 & k_3 & -\omega_3/2 & -\omega_4/2 & -\omega_5/2 & -\omega_6/2 \\ 0 & -\omega_1/2 & -\omega_3/2 & \Xi & 0 & 0 & 0 \\ 0 & -\omega_2/2 & -\omega_4/2 & 0 & \Xi & 0 & 0 \\ 0 & 0 & -\omega_5/2 & 0 & 0 & \Xi & 0 \\ 0 & 0 & -\omega_6/2 & 0 & 0 & 0 & \Xi \end{bmatrix}; z = [z_1,\ z_2, z_3]^T$$

Thus, we can rewrite (56) according to the following form

$$\dot{V}_4 \leq -\begin{bmatrix} z & \varepsilon \end{bmatrix}^T \Gamma \begin{bmatrix} z & \varepsilon \end{bmatrix} + \Upsilon \tag{57}$$

Since Γ is a positive definite matrix, we can write

$$\begin{aligned} \dot{V}_4 \leq -\lambda_{\min}(\Gamma)\left(\|z\|^2 + \|\varepsilon\|^2\right) + \Upsilon \leq -\lambda_{\min}(\Gamma)\left(\|z\|^2 + \tfrac{1}{\lambda_{\max}(P)}\varepsilon^T P \varepsilon\right) + \Upsilon \\ \leq -\beta V_4 + \Upsilon \end{aligned} \tag{58}$$

where $\lambda_{\min}(\Gamma)$ is the minimal eigenvalue of the matrix Γ and $\lambda_{\max}(P)$ is the maximal eigenvalue of the matrix P.

Multiplying (58) by $e^{\beta t}$ on both sides and integrating, we obtain

$$e^{\beta t}\dot{V}_4 + \beta e^{\beta t} V_4 \leq e^{\beta t}\Upsilon \tag{59}$$

$$\int_0^t \left(e^{\beta t} V_4\right)' dt \leq \Upsilon \int_0^t e^{\beta t} dt \tag{60}$$

$$V_4(t) \leq \left(V_4(0) - \frac{\Upsilon}{\beta}\right)e^{-\beta t} + \frac{\Upsilon}{\beta} \leq V_4(0)e^{-\beta t} + \frac{\Upsilon}{\beta} \tag{61}$$

Remark 5. *According to (61), the tracking errors z_i and ε_i are bounded, the system variables x_i and their estimation are also bounded with the control gains and observer bandwidth in a finite time. Thus, the proposed control scheme can approximate the unmodeled dynamics of the suspension system.*

Remark 6. *Adaptive backstepping control with PPF and ESO is developed to stabilize the vertical displacement of the chassis. Although the parametric uncertainties can be compensated, the unknown parameter caused by the different masses of passengers still affects the output performance of the suspension system. This remained problem will be solved by the NNs in the following section.*

3.4. Adaptive NNs Backstepping Controller Design with PPF and ESO

In a real vehicle system, the total weight of the sprung mass m_s is a flexible variable that can be changed due to different passenger masses. Therefore, the system model of the sprung mass (14) contains some parametric uncertainties. Moreover, the damping characteristic of air springs cannot be exactly modeled and is often ignored in the pneumatic system. In step 3 of section III.C, we can see that the virtual control α_2 contains the unknown parameter of passenger masses. In this section, the Equation (40) can be rewritten without using ESO as follows

$$\alpha_2 = -z_1\varsigma + \dot{\alpha}_1 + \frac{1}{m_{ch}}\left[k_{sp}(x_1 - x_3) + c_a(x_2 - x_4)\right] - k_2 z_2 \tag{62}$$

The uncertain function can be defined as

$$f(X) = \frac{1}{m_s}[k_s(x_1 - x_3) + c_a(x_2 - x_4)] \tag{63}$$

Because the chassis parameter is unknown, $f(X)$ is an unknown function that will affect system performance. Although these unknown functions cannot be solved directly by a normal controller, neural networks can be used to approximate them. Therefore, RBFNNs are then applied to compensate for the unknown function in this study.

Lemma 3. [50]. *Based on the RBFNNs approximation, the unknown continuous function* $f(X)$ *can be estimated by*

$$f(X) = W_h^T S(X) + \eta(X) \tag{64}$$

where $W_h = [w_1, w_2, \ldots, w_n]^T \in R^n$ *is called the weight vector,* $S(X) = [s_1(X), s_2(X), \ldots, s_n(X)]^T$ *represents the Gaussian function vector,* $\eta(X)$ *denotes the approximation error,* $n > 1$ *defines the node number, and* X *is the input vector.*

Gaussian basis function can be expressed as

$$S_i(X) = \exp\left(-\frac{\|X - \zeta_i\|^2}{\sigma_i^2}\right), \; i = 1, 2, \ldots, n \tag{65}$$

where σ_i and ζ_i are the width and center of the basic function.

According to [51], for any continuous function $f(X)$ and an arbitrary $\delta > 0$, there are the RBFNNs $W_h^T S(X)$ that are satisfying $\left|W_h^T S(X) - f(X)\right| \leq \delta$.

Therefore, the virtual control α_2 in (40) will be proposed again as follows

$$\alpha_2 = -z_1\varsigma + \dot{\alpha}_1 - \hat{W}_h^T S(X) - k_2 z_2 \tag{66}$$

where the input vector is selected by $X = [x_1, x_2, x_3, x_4]^T$.

We design an adaptive law based on an adaptive algorithm

$$\dot{\hat{W}}_h = \Lambda_h\left[S(X)z_2 - \delta_h \hat{W}_h\right] \tag{67}$$

where $\Lambda_h > 0$ and $\delta_h > 0$ are the constant gains of the adaptive estimation law. The controller scheme can be described in Figure 2.

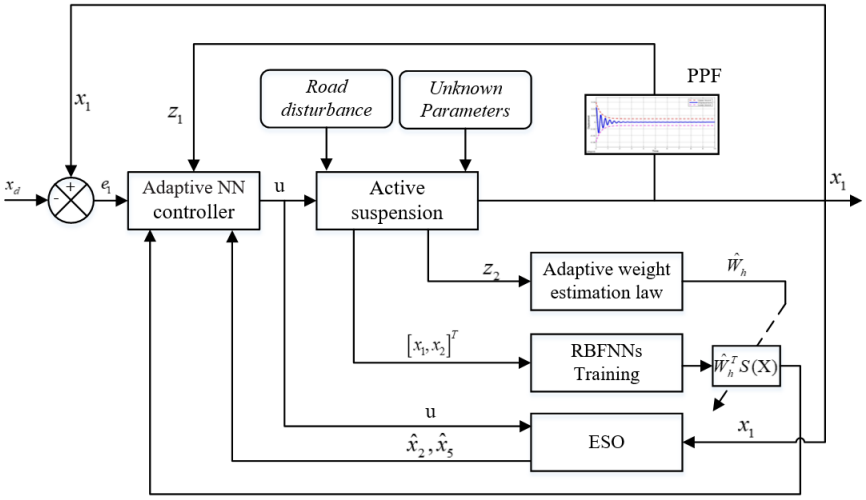

Figure 2. Structure diagram of adaptive neural backstepping controller design with PPF and ESO.

Theorem 2. *Considering the pneumatic vehicle suspension design (14), the adaptive NNs backstepping controller is proposed by (33), (46), (66) together with the adaptation law (67). Then, an adaptive output feedback control scheme is developed based on tuning the bandwidth parameters* ω_0 *of ESO and the constant gains* Λ_h, δ_h, ζ_i, σ_i *of RBFNNs estimation. Besides, the boundary*

parameters $\underline{\kappa}, \overline{\kappa}, \rho_0$ of PPF are chosen to meet the initial condition $-\underline{\kappa}\rho(t) < x_1 < \overline{\kappa}\rho(t)$. This is to ensure that the semi-global stability of the system is guaranteed, i.e., the system states and estimation errors converge asymptotically to a small set around zero. Thus, the chassis displacement is ensured within the specified PPF boundary.

Proof. Using ESO and NNs estimation, the candidate Lyapunov functions for the whole closed-loop control system are chosen again by

$$V = V_3 + \frac{1}{2}\varepsilon^T P\varepsilon + \frac{1}{2}\widetilde{W}_h^T \Lambda_h^{-1} \widetilde{W}_h \tag{68}$$

where the error weight vector is designed as $\widetilde{W}_h = W_h - \hat{W}_h$.

Then, the time derivative of V is obtained

$$\dot{V} = \dot{V}_3 + \frac{1}{2}\dot{\varepsilon}^T P\varepsilon + \frac{1}{2}\varepsilon^T P\dot{\varepsilon} - \widetilde{W}_h^T \Lambda_h^{-1} \dot{\hat{W}}_h \tag{69}$$

Substituting (64) and (66) into (39), we can rewrite the time derivative of V_2 as follows

$$\dot{V}_2 = -k_1 z_1^2 + z_2\Big[z_3 - k_2 z_2 + \widetilde{W}_h^T S(X) + \eta(X) + d_0 + d(t)\Big] \tag{70}$$

Based on (47) and (70), we can rewrite

$$\begin{aligned}\dot{V} = &-k_1 z_1^2 + z_2 \widetilde{W}_h^T S(X) + z_2\eta(X) + z_2(d_0 + d(t)) + z_3\widetilde{f}_2 + z_3\omega_0^3\varepsilon_6 \\ &+z_3(k_1k_2+1)\omega_0\varepsilon_2 + k_3 z_3\omega_0^2\varepsilon_5 + \tfrac{1}{2}\dot{\varepsilon}^T P\varepsilon + \tfrac{1}{2}\varepsilon^T P\dot{\varepsilon} - \widetilde{W}_h^T\Lambda_h^{-1}\dot{\hat{W}}_h - k_2 z_2^2 - k_3 z_3^2\end{aligned} \tag{71}$$

Substituting (26) and (67) into (71), we have:

$$\begin{aligned}\dot{V} = &-k_1 z_1^2 - k_2 z_2^2 + z_2(d_0 + d(t)) + z_2\widetilde{W}_h^T S(X) - k_3 z_3^2 + z_2\eta(X) - \widetilde{W}_h^T\left[S(X)z_2 - \delta_h\hat{W}_h\right] \\ &+\varepsilon^T PM\tfrac{d_0+d(t)}{\omega_0} + z_3\widetilde{f}_2 + z_3\omega_0^3\varepsilon_6 + z_3(k_1k_2+1)\omega_0\varepsilon_2 + k_3 z_3\omega_0^2\varepsilon_5 \ - \omega_0\|\varepsilon\|^2 \\ &+\varepsilon^T PM\tfrac{\widetilde{f}_1}{\omega_0} + \varepsilon^T PN\tfrac{\widetilde{f}_2}{\omega_0^2} + \varepsilon^T PN\tfrac{\widetilde{g}u}{\omega_0^2} + \varepsilon^T PK\tfrac{h(t)}{\omega_0^3}\end{aligned} \tag{72}$$

According to Young's inequality, it yields

$$\begin{aligned}z_2\eta(X) &\le \tfrac{z_2^2}{2} + \tfrac{\eta^2(X)}{2} \\ \widetilde{W}_h^T W &\le \tfrac{\widetilde{W}_h^T\widetilde{W}_h}{2} + \tfrac{W_h^T W_h}{2}\end{aligned} \tag{73}$$

Applying (51), (52) and (73) into (72), we can write

$$\begin{aligned}\dot{V} \le &-k_1 z_1^2 - k_2 z_2^2 - k_3 z_3^2 + \tfrac{1}{2}z_2^2 + \tfrac{1}{2}(|d_0|_{\max} + |d(t)|_{\max})^2 + \tfrac{1}{2}z_2^2 - \tfrac{\delta_h\|\widetilde{W}_h\|^2}{2} + \tfrac{\delta_h\|W_h\|^2}{2} \\ &+\tfrac{\eta^2(X)}{2} + \omega_0^3\varepsilon_6 z_3 + \tfrac{1}{2}\|\varepsilon\|^2 + (c_3|\varepsilon_1| + c_4|\varepsilon_2| + c_5|\varepsilon_5|)z_3 + (k_1k_2+1)\omega_0\varepsilon_2 z_3 \\ &+k_3\omega_0^2\varepsilon_5 z_3 + \tfrac{\phi_3^2}{2\omega_0^6}|h(t)|_{\max}^2 + \tfrac{1}{2}\|\varepsilon\|^2 + \tfrac{\phi_2^2}{2\omega_0^2}(|d_0|_{\max} + |d(t)|_{\max})^2 \\ &+\left(-\omega_0 + \tfrac{\phi_1(c_1+c_2)}{\omega_0} + \tfrac{\phi_2(c_3+c_4+c_5)}{\omega_0^2} + \tfrac{\phi_2 c_6}{\omega_0^2}|u|_{\max}\right)\|\varepsilon\|^2\end{aligned} \tag{74}$$

We can set the total upper-bounded of these states as

$$\Delta = \frac{1}{2}(|d_0|_{\max} + |d(t)|_{\max})^2 + \frac{\phi_2^2}{2\omega_0^2}(|d_0|_{\max} + |d(t)|_{\max})^2 + \frac{\phi_3^2}{2\omega_0^6}|h(t)|_{\max}^2 + \frac{\delta_h\|W_h\|^2}{2} + \frac{\eta^2(X)}{2}$$

$$\Pi = \omega_0 - \frac{\phi_1(c_1+c_2)}{\omega_0} - \frac{\phi_2(c_3+c_4+c_5)}{\omega_0^2} - \frac{\phi_2 c_6}{\omega_0^2}|u|_{\max} - 1$$

As a result, inequality (74) can be written by

$$\dot{V} \leq -k_1 z_1^2 - (k_2 - 1) z_2^2 - k_3 z_3^2 - \Pi \|\varepsilon\|^2 - \frac{\delta_h \|\widetilde{W}_h\|^2}{2} + c_3 |\varepsilon_1| z_3 + (k_1 k_2 + c_4 + 1)\omega_0 |\varepsilon_2| |z_3| + \left(c_5 + k_3 \omega_0^2\right) |\varepsilon_5| |z_3| + \omega_0^3 |\varepsilon_6| |z_3| + \Delta \tag{75}$$

Set $\xi_1 = c_3$; $\xi_2 = (k_1 k_2 + c_4 + 1)\omega_0$; $\xi_3 = c_5 + k_3 \omega_0^2$; $\xi_4 = \omega_0^3$ and define a new matrix Ω

$$\Omega = \begin{bmatrix} k_1 & 0 & 0 & 0 & 0 & 0 & 0 & 0 \\ 0 & k_2 - 1 & 0 & 0 & 0 & 0 & 0 & 0 \\ 0 & 0 & k_3 & -\xi_1/2 & -\xi_2/2 & -\xi_3/2 & -\xi_4/2 & 0 \\ 0 & 0 & -\xi_1/2 & \Pi & 0 & 0 & 0 & 0 \\ 0 & 0 & -\xi_2/2 & 0 & \Pi & 0 & 0 & 0 \\ 0 & 0 & -\xi_3/2 & 0 & 0 & \Pi & 0 & 0 \\ 0 & 0 & -\xi_4/2 & 0 & 0 & 0 & \Pi & 0 \\ 0 & 0 & 0 & 0 & 0 & 0 & 0 & \delta_h/2 \end{bmatrix}$$

We can rewrite (75) as follows

$$\dot{V} \leq -\begin{bmatrix} z & \varepsilon & \widetilde{W}_h \end{bmatrix}^T \Omega \begin{bmatrix} z & \varepsilon & \widetilde{W}_h \end{bmatrix} + \Delta \tag{76}$$

Since Ω is a positive definite matrix, we can obtain (76) as follows

$$\dot{V} \leq -\lambda_{\min}(\Omega) \left(\|z\|^2 + \|\varepsilon\|^2 + \frac{\delta_h \|W_h\|^2}{2} \right) + \Delta \tag{77}$$

And we can obtain (77) as follows

$$\dot{V} \leq -\lambda_{\min}(\Omega) \left(\|z\|^2 + \frac{1}{\lambda_{\max}(P)} \varepsilon^T P \varepsilon + \delta_h \Lambda_h \frac{\Lambda_h^{-1} \|W_h\|^2}{2} \right) + \Delta \leq -\Phi V + \Delta \tag{78}$$

where $\lambda_{\min}(\Omega)$ is the minimal eigenvalue of the matrix Ω and $\lambda_{\max}(P)$ is the maximal eigenvalue of the matrix P.

Multiplying (78) by $e^{\Phi t}$ on both sides and integrating, we obtain

$$e^{\Phi t} \dot{V} + \Phi e^{\Phi t} V \leq e^{\Phi t} \Delta \tag{79}$$

$$\int_0^t \left(e^{\Phi t} V \right)' dt \leq \Delta \int_0^t e^{\Phi t} dt \tag{80}$$

$$V(t) \leq \left(V(0) - \frac{\Delta}{\Phi} \right) e^{-\Phi t} + \frac{\Delta}{\Phi} \leq V(0) e^{-\Phi t} + \frac{\Delta}{\Phi} \tag{81}$$

According to (68), the following conditions are satisfied

$$|z_i| \leq \sqrt{2 \left(V(0) e^{-\Phi t} + \frac{\Delta}{\Phi} \right)}, \; i = 1, 2, 3 \tag{82}$$

Obviously, we can see that the error signals can be bounded to a small zero neighborhood by adjusting the control parameters as $t \to \infty$. Thus, the transformed error z_1 is bounded and then $-\underline{\kappa} < S(z_1) < \overline{\kappa} \forall z_1 \in R$ is guaranteed. It is illustrated that $-\underline{\kappa} \rho(t) < e_1 < \overline{\kappa} \rho(t) \forall t > 0$. It means that the vertical displacement of the chassis is conserved within the small predefined constraints.

Remark 7. *The estimation tracking errors ε and $\widetilde{W}_h$ are bounded, so the system states x_i and their estimation values are also limited to a monotonous decrease with the observer bandwidth in*

a finite time. Thus, the observer bandwidth and constant gains of adaptive estimation law can be adjusted to guarantee the dynamic behavior of the system in the presence of unknown parameters and external disturbance.

3.5. Road Holding and Handling Stability Analysis

In the above analysis, the guarantee for sprung mass displacement x_1 to remain within the prescribed performance boundaries has been obtained, i.e., the first performance of ride comfort is achieved. In this section, two objectives of road holding and handling stability can be ensured by adjusting the control parameters appropriately.

To analyze the road holding and handling stability of suspension systems, we suppose that the tracking errors $e_1 = 0$ and $z_2 = 0$ are bounded, i.e., the vertical displacement x_1 and speed x_2 converge to a small zero neighborhood. For this purpose, we focus the system states of the unsprung mass with x_3 and x_4 in the system (3). Then, substituting (3) into (63), we obtain

$$\dot{X} = EX + FZ_0 + Z \tag{83}$$

where $X = \begin{bmatrix} x_3 \\ x_4 \end{bmatrix}$; $E = \begin{bmatrix} 0 & 1 \\ -\frac{k_t}{m_u} & -\frac{c_t}{m_u} \end{bmatrix}$; $F = \begin{bmatrix} 0 & 0 \\ \frac{k_t}{m_u} & \frac{c_t}{m_u} \end{bmatrix}$; $Z_0 = \begin{bmatrix} z_r \\ \dot{z}_r \end{bmatrix} Z = \begin{bmatrix} 0 \\ \psi \end{bmatrix}$; $\psi = \frac{m_s}{m_u}\left(W_h^T S(X) + \eta(X)\right) + \frac{1}{m_u}(-m_s x_5 - m_s d_0)$.

Besides, the tracking errors z_1, z_2, and z_3 with be bounded according to (82), so ψ is bounded and there exists a constant $\overline{\psi}$ such that $\|\psi\| \leq \overline{\psi}$.

Then, the Lyapunov function is selected as

$$V_a = X^T P X \tag{84}$$

where P is a positive definite symmetric matrix.

Then, we can describe the time derivative of V as follows

$$\dot{V}_a = \dot{X}^T P X + X^T P \dot{X} \tag{85}$$

Substituting (83) into (85), we have

$$\dot{V}_a = X^T \Big(E^T P + PE\Big) X + 2X^T P F Z_0 + 2X^T P Z \tag{86}$$

There exists a positive definite symmetric matrix $Q > 0$ which is chosen to satisfy the Lyapunov equation $E^T P + PE = -Q$. Based on Young's inequality theorem for two nonnegative real numbers a and b, we have $ab \leq a^2/2\gamma_i + b^2\gamma_i/2$. Therefore, we can apply these results for $2X^T P F Z_0$ and $2X^T P Z$ as follows

$$\begin{aligned} 2X^T P F Z_0 &\leq \tfrac{1}{\gamma_1} X^T P F F^T P X + \gamma_1 Z_0^T Z_0 \\ 2X^T P Z &\leq \tfrac{1}{\gamma_2} X^T P P X + \gamma_2 Z^T Z \end{aligned} \tag{87}$$

where $\gamma_i > 0$, $i = 1, 2$ are the control parameters.

Applying (87) into (86), we obtain

$$\dot{V}_a \leq -\left[\lambda_{\min}\left(P^{\frac{-1}{2}} Q P^{\frac{-1}{2}}\right) - \frac{1}{\gamma_1}\lambda_{\max}\left(P^{\frac{1}{2}} F F^T P^{\frac{1}{2}}\right) - \frac{1}{\gamma_2}\lambda_{\max}(P)\right] V_a + \gamma_1 Z_0^T Z_0 + \gamma_2 Z^T Z \tag{88}$$

where $\lambda_{\min}$ and $\lambda_{\max}$ denote the minimal and maximal eigenvalues of the matrix.

Select the appropriate matrix P, Q so that

$$\gamma_1 > 2\frac{\lambda_{\max}\left(P^{\frac{1}{2}} F F^T P^{\frac{1}{2}}\right)}{\lambda_{\min}\left(P^{\frac{-1}{2}} Q P^{\frac{-1}{2}}\right)};\ \gamma_2 > 2\frac{\lambda_{\max}(P)}{\lambda_{\min}\left(P^{\frac{-1}{2}} Q P^{\frac{-1}{2}}\right)} \tag{89}$$

From (89), there exist γ and ν that satisfy

$$\gamma \geq \lambda_{\min}\left(P^{\frac{-1}{2}} Q P^{\frac{-1}{2}}\right) - \frac{1}{\gamma_1}\lambda_{\max}\left(P^{\frac{1}{2}} F F^T P^{\frac{1}{2}}\right) - \frac{1}{\gamma_2}\lambda_{\max}(P) \tag{90}$$

$$\nu \geq \gamma_1 Z_0^T Z_0 + \gamma_2 Z^T Z \tag{91}$$

Then, the inequality (88) can be rewritten by

$$\dot{V}_a \leq -\gamma V_a + \nu \tag{92}$$

We can integrate both sides of (92) to get

$$V_a \leq \left(V_a(0) - \frac{\nu}{\gamma}\right)e^{-\gamma t} + \frac{\nu}{\gamma} \leq V_a(0)e^{-\gamma t} + \frac{\nu}{\gamma} \tag{93}$$

Obviously, we can know

$$|x_i(t)| \leq \sqrt{\left(V_a(0)e^{-\gamma t} + \frac{\nu}{\gamma}\right)/\lambda_{\min}(P)}\,,\ i\ =\ 3,4 \tag{94}$$

Based on the relative tire force condition in (12), the tire forces F_{st} and F_{dt} can be calculated as

$$\begin{aligned} F_{st}(z_u, z_r, t) &\leq k_t\sqrt{\left(V_a(0)e^{-\gamma t} + \tfrac{\nu}{\gamma}\right)/\lambda_{\min}(P)} + k_t\|z_r\|_\infty \\ F_{dt}(z_u, z_r, t) &\leq c_t\sqrt{\left(V_a(0)e^{-\gamma t} + \tfrac{\nu}{\gamma}\right)/\lambda_{\min}(P)} + c_t\left\|\dot{z}_r\right\|_\infty \end{aligned} \tag{95}$$

Substituting (95) into (2), we can obtain

$$|F_{st} + F_{dt}| \leq (k_t + c_t)\sqrt{\left(V_a(0)e^{-\gamma t} + \frac{\nu}{\gamma}\right)/\lambda_{\min}(P)} + k_t\|z_r\|_\infty + c_t\left\|\dot{z}_r\right\|_\infty \tag{96}$$

Based on (96) the RTF constraints are guaranteed by selecting the design parameters γ_1, γ_2, and matrix P so that $|F_{st} + F_{dt}| \leq (m_s + m_u)g$ is ensured.

Besides, the suspension deflection condition (13) can be expressed as

$$|z_s - z_u| \leq |x_1| + |x_3| \leq \overline{\kappa}\rho(0) + \sqrt{\left(V_a(0)e^{-\gamma t} + \frac{\nu}{\gamma}\right)/\lambda_{\min}(P)} \tag{97}$$

Then the suspension deflection constraints will be ensured by selecting the PPF coefficients $\overline{\kappa}$, $\underline{\kappa}$, $\rho(0)$ and design parameters γ_1, γ_2, P so that $|z_s - z_u| \leq z_R$.

Based on the above analysis, we can conclude that the three objectives of suspension performance requirements are improved by designing initial conditions and suitable control parameters, i.e., the mechanical structure and safety condition of the pneumatic active suspension are satisfied.

Remark 8. *Adaptive backstepping control based on PPF can guarantee not only the steady-state error limitations but also the transient response of chassis displacement. Moreover, by selecting the appropriate PPF and feedback control parameters, the developed method can enhance the suspension requirements.*

4. Simulation Results and Discussion

4.1. Simulation Description

The comparative simulations of the proposed control scheme are evaluated in comparison with passive suspension, traditional backstepping, and ESO backstepping to verify the effectiveness of the control design in this study. The passenger comfort of the vehicle suspension is evaluated by the human body's sensitivity to acceleration. Moreover, the ride comfort is considered by the peak and the root mean square (RMS) values of sprung mass acceleration. For this evaluation, a filter is proposed in [52] to find the RMS acceleration during the simulation process.

$$W(s) = \frac{80.03s^2 + 989s + 0.02108}{s^3 + 78.92s^2 + 2412s + 5614} \tag{98}$$

Furthermore, the simulation results of RSD and RTF are analyzed to prove two objectives of driving safety and suspension deflection. The main parameters of pneumatic active suspension are listed in Table 1.

Table 1. Pneumatic vehicle suspension parameters.

Parameter	Value	Unit
m_s	$550 \pm 100\sin(\pi t)$	kg
m_u	60	kg
k_s	16,000	Nm^{-1}
k_t	145,000	Nm^{-1}
c_a	2300	Nsm^{-1}
c_t	1100	Nsm^{-1}
z_R	0.04	m
z_{as0}	0.18	m
R	287.5	$J{\cdot}kg^{-1}{\cdot}K^{-1}$
A_{as}	0.0047	m^2
κ	1.4	-
T	293.15	K

The sin road profile is chosen for these simulations $z_r = 0.02\sin(4\pi t)$. The initial condition of the system states are set by $x_1(0) = 0.05\ (m)$, $x_2(0) = x_3(0) = x_4(0) = 0\ (m)$, and $x_5(0) = 0.5 \times 10^5\ (Pa)$.

The prescribed performance constraints are given by $\rho_0 = 0.058$, $\rho_\infty = 0.0029$, $\varphi = 1.5$ and design parameters $\underline{\kappa} = 0.98$, $\overline{\kappa} = 0.98$. The bandwidth of the ESO system is chosen by $\omega_0 = 150$. Moreover, the constant gains of the adaptive estimation law of RBFNNs are selected as $\Lambda_h = 50$, $n = 21$, and $\delta_h = 30$. The comparison of the control parameters is given in Table 2.

Table 2. Control parameters.

Controller	Parameter
Backstepping	$k_1 = 100,\ k_2 = 20,\ k_3 = 5$
ESO	$k_1 = 100,\ k_2 = 20,\ k_3 = 5$ $\omega_0 = 150$
Proposed	$k_1 = 100,\ k_2 = 20,\ k_3 = 5$ $\omega_0 = 150,\ n = 21,\ \Lambda_h = 50$ $\sigma = 0.01, \zeta = [-2, 0.1, 2]$

4.2. Simulation Results

The simulation results of sprung mass displacement and acceleration, tracking error of sprung mass displacement, RSD, RTF, and control signals of passive suspension, traditional backstepping, and ESO backstepping, and developed control are displayed in Figures 3–9.

With the developed control, the ride comfort is strongly improved because the sprung mass acceleration and displacement have been reduced. By introducing a PPF, the proposed control can guarantee the displacement of sprung mass convergence in a finite time to get the ride comfort as shown in Figure 3. Besides, we can see that the time of zero convergence for the error signals e_1 is about $t = 1.2\ (s)$ as shown in Figure 4. Moreover, passenger comfort is strongly improved thanks to the developed method because root mean square values of chassis acceleration are decreased by 69.43% as shown in Figure 5.

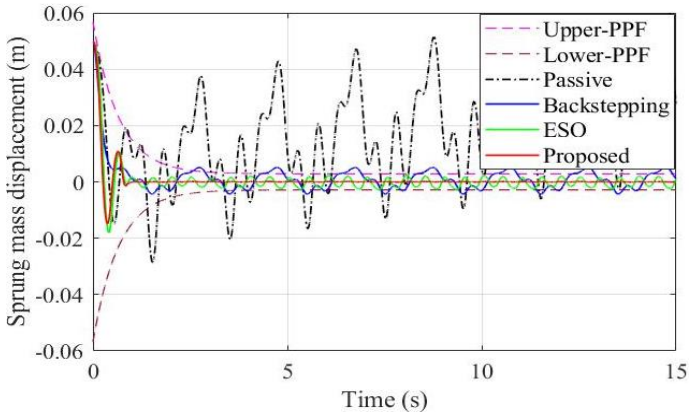

Figure 3. Simulation result of sprung mass displacement.

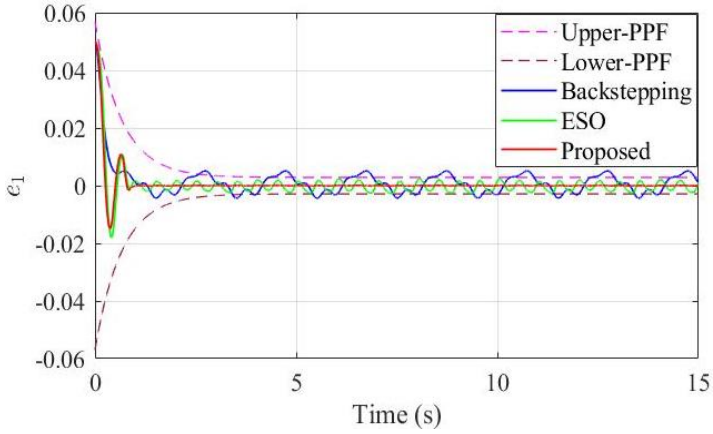

Figure 4. Tracking error of sprung mass displacement.

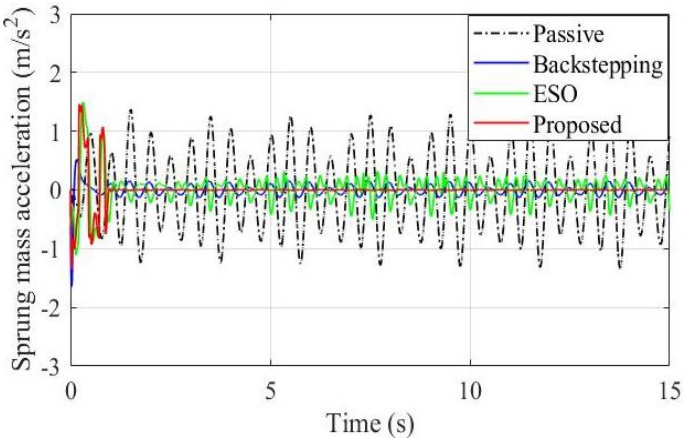

Figure 5. Simulation result of sprung mass acceleration.

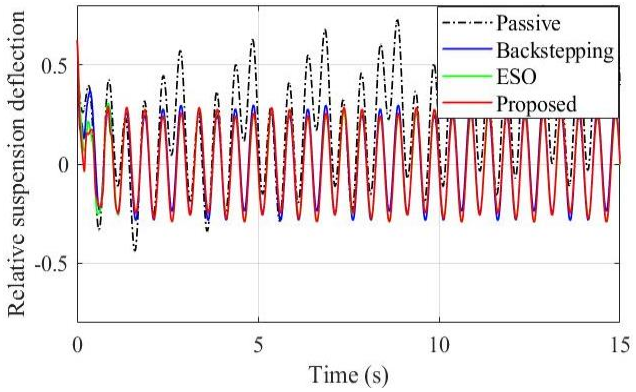

Figure 6. Relative suspension deflection.

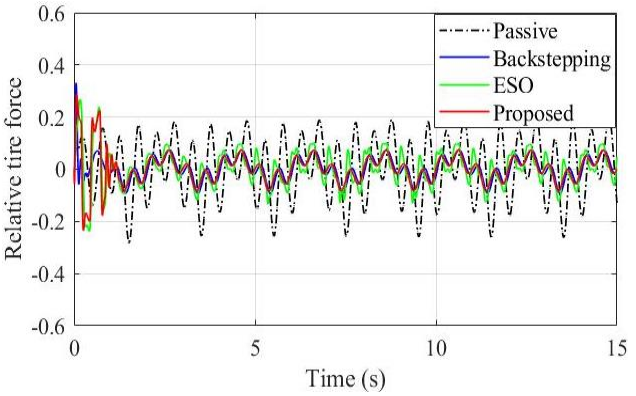

Figure 7. Relative tire force.

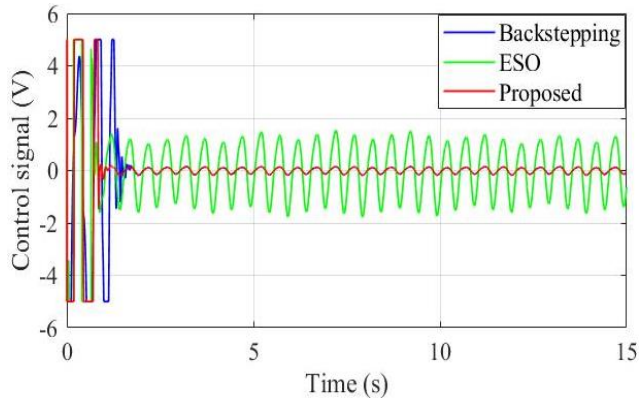

Figure 8. Control signal (V).

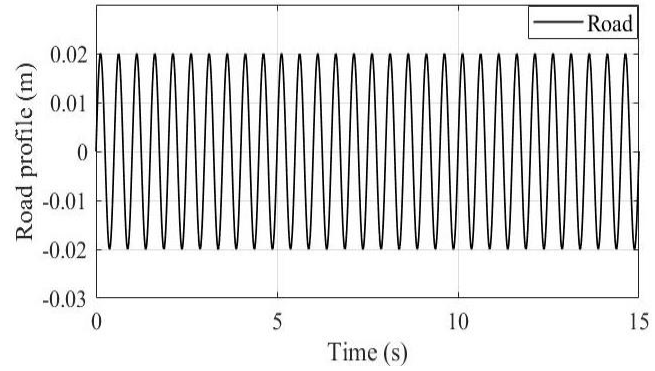

Figure 9. Road profile.

In comparison with passive suspension, the sprung mass displacement can reduce with traditional backstepping but there have some high peak values because of external disturbance. Moreover, the developed method can guarantee the sprung mass deflection, which is smaller than traditional backstepping and passive suspension. From Figure 6, the proposed control gives the magnitude of the RSD smaller than the conventional backstepping and passive, and this RSD is guaranteed within limits. The proposed control design can improve passenger comfort by selecting the sprung mass vertical displacement under the exogenous road disturbance while keeping the result of RSD within the limit value. It is also possible to see from the RTF values in Figure 7 that dynamic stroke constraints are satisfied because the limit is less than 1. Although both ESO backstepping and proposed control can ensure that dynamic and steady tracking errors are limited in the PPF constraints, only the proposed control can converge the system state x_1 in a small neighborhood of the origin. Under the effect of parametric uncertainties, the ESO backstepping needs to consume more than the proposed control to compensate for this model error as shown in Figure 8.

Figures 10–12 plotted the estimation results of system states under the effect of external disturbances and their estimation errors. The simulation results show that the ESO can estimate system states accurately. Because the stiffness coefficient of the air spring depends on the rubber behavior under vertical displacement, the disturbance observer can estimate the influent of air spring stiffness and unmodeled dynamic of air pressure to guarantee the suspension performance. Although estimation errors exist between the real external disturbance and estimated value, they can be as low as possible by the approximate selection of observer parameters. The model estimation result of adaptive NNs law is shown in Figure 13. With the RBFNNs, the developed control approach can provide a good tracking performance for pneumatic vehicle suspension. Simulation results show that the proposed control with the PPF is able to satisfy the performance requirements of the pneumatic suspension more than the traditional backstepping control.

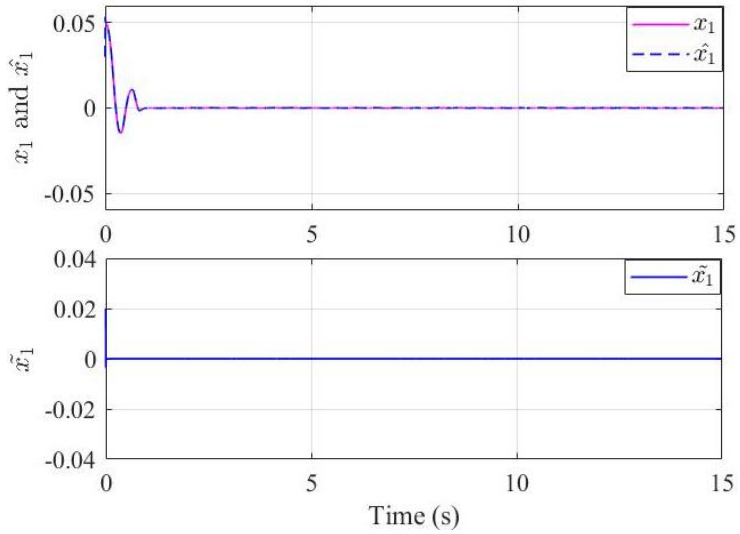

Figure 10. Estimation of x_1 and estimation error.

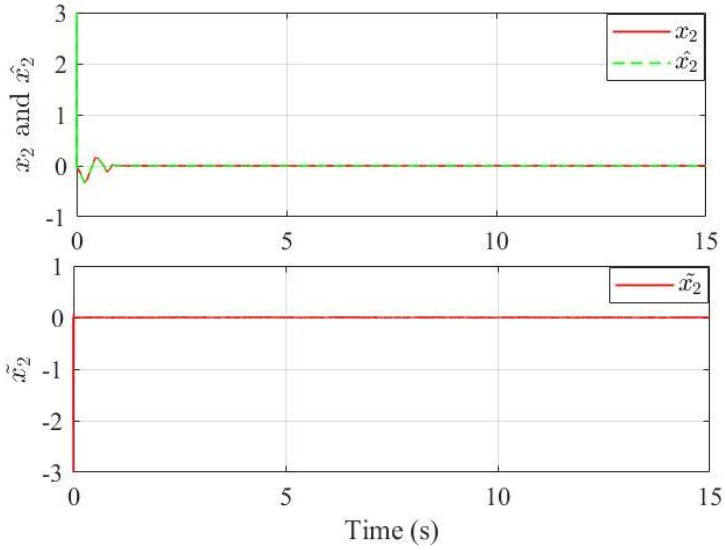

Figure 11. Estimation of x_2 and estimation error.

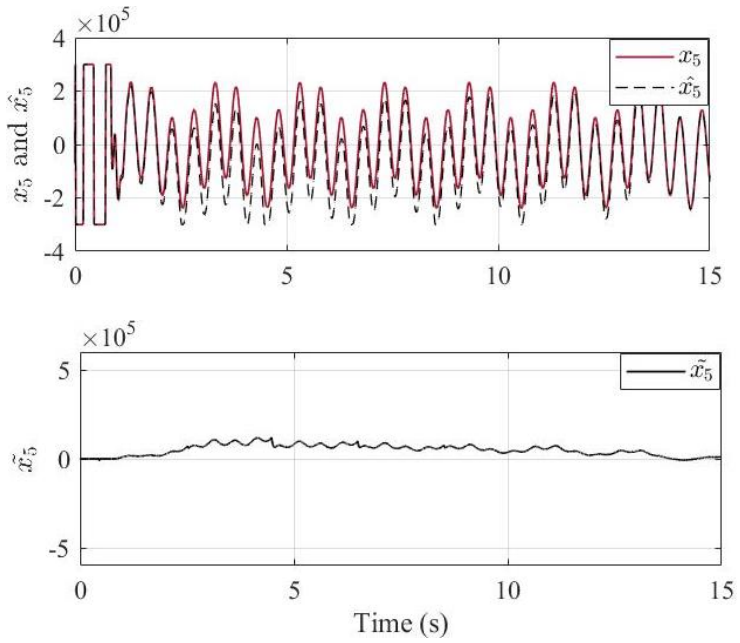

Figure 12. Estimation of x_5 and estimation error.

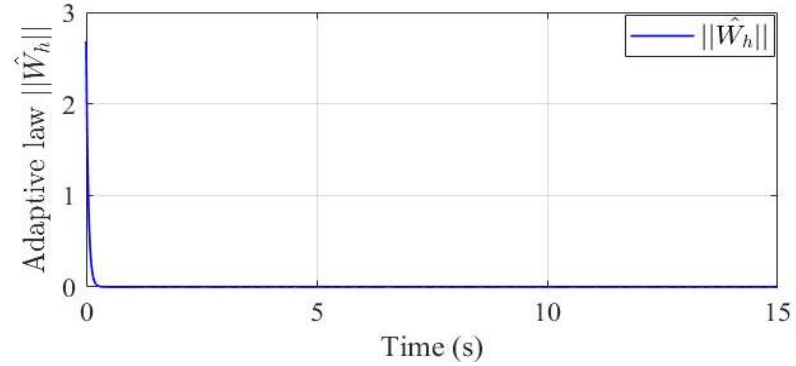

Figure 13. Adaptive law.

5. Conclusions

In this study, an ESO-Based Adaptive NNs Backstepping Control with PPF was proposed for pneumatic vehicle suspension under the effect of parametric uncertainties. The stability problem for suspension systems subject to uncertain parameters, external disturbances, and the unmodeled dynamic was solved in this paper. The nonlinear dynamics and unknown parameters are estimated by the ESO and the uncertainty continuous function of the car-body mass is compensated by RBFNNs. An improved backstepping scheme based on PPF constraints is developed for an air bellow actuator to guarantee the system stability and steady-state tracking error of sprung mass vertical displacement. When the observer bandwidth of ESO was chosen, the convergence of the ESO and the output tracking are established in this work. Moreover, the proposed controller-based adaptive NNs can be more efficient than traditional backstepping control. Finally, the system stability of the developed control is guaranteed by applying the Lyapunov theory. Simulation results of RMS of acceleration values decreased by 69.43% when using the proposed control. In conclusion, this proposed control scheme is not only effective to enhance the passenger comfort but also to guarantee the road holing, which can be considered as a promising method for the vehicle industry.

Author Contributions: K.K.A. is the funding supervisor and project manager, and he reviewed and edited the manuscript. C.M.H. investigated, analyzed, created MATLAB software, set up the simulation, and wrote the main content of the paper. All authors have read and agreed to the published version of the manuscript.

Funding: This work was supported in part by Basic Science Program through the National Research Foundation of Korea (NRF) funded by the Ministry of Science and ICT, South Korea under Grant NRF 2020R1A2B5B03001480, and in part by Regional Innovation Strategy (RIS) through the National Research Foundation of Korea (NRF) funded by the Ministry of Education (MOE) under Grant 2021RIS-003.

Institutional Review Board Statement: Not applicable.

Informed Consent Statement: Not applicable.

Data Availability Statement: Not applicable.

Conflicts of Interest: The author declares no conflict of interest.

References

1. Pusadkar, U.S.; Chaudhari, S.D.; Shendge, P.; Phadke, S. Linear disturbance observer based sliding mode control for active suspension systems with non-ideal actuator. *J. Sound Vib.* **2018**, *442*, 428–444. [CrossRef]
2. Hamza, A.; Yahia, N.B. Artificial neural networks controller of active suspension for ambulance based on ISO standards. *Proc. Inst. Mech. Eng. Part D J. Automob. Eng.* **2022**, *237*, 34–47. [CrossRef]
3. Gysen, B.L.J.; Paulides, J.J.H.; Janssen, J.L.G.; Lomonova, E.A. Active Electromagnetic Suspension System for Improved Vehicle Dynamics. *IEEE Trans. Veh. Technol.* **2010**, *59*, 1156–1163. [CrossRef]
4. Hamza, A. Development of a Model to Assist the Design of Active Mechanisms for Suspension of Heavy-Duty Trucks According to a Multi-Criteria Approach. Ph.D. Thesis, National School of Engineering of Tunis (ENSIT), University of Tunis, Tunis, Tunisia, 2021.
5. Hamza, A. *Development of a Design Support Model Active Suspension Mechanisms for Heavy Trucks Using a Multi-Criteria Approach*; Our Knowledge Publishing: Maharashtra, India, 2022.
6. Haiping, D.; Nong, Z. Fuzzy Control for Nonlinear Uncertain Electrohydraulic Active Suspensions with Input Constraint. *IEEE Trans. Fuzzy Syst.* **2009**, *17*, 343–356. [CrossRef]
7. Van der Sande, T.; Gysen, B.; Besselink, I.; Paulides, J.; Lomonova, E.; Nijmeijer, H. Robust control of an electromagnetic active suspension system: Simulations and measurements. *Mechatronics* **2013**, *23*, 204–212. [CrossRef]
8. Holtz, M.W.; van Niekerk, J.L. Modelling and design of a novel air-spring for a suspension seat. *J. Sound Vib.* **2010**, *329*, 4354–4366. [CrossRef]
9. He, L.; Xu, W.; Bu, W.; Shi, L. Dynamic analysis and design of air spring mounting system for marine propulsion system. *J. Sound Vib.* **2014**, *333*, 4912–4929. [CrossRef]

10. Chen, J.-J.; Yin, Z.-H.; Rakheja, S.; He, J.-H.; Guo, K.-H. Theoretical modelling and experimental analysis of the vertical stiffness of a convoluted air spring including the effect of the stiffness of the bellows. *Proc. Inst. Mech. Eng. Part D J. Automob. Eng.* **2017**, *232*, 547–561. [CrossRef]
11. Hyunsup, K.; Hyeongcheol, L. Height and Leveling Control of Automotive Air Suspension System Using Sliding Mode Approach. *IEEE Trans. Veh. Technol.* **2011**, *60*, 2027–2041. [CrossRef]
12. Ma, X.; Wong, P.K.; Zhao, J.; Zhong, J.-H.; Ying, H.; Xu, X. Design and Testing of a Nonlinear Model Predictive Controller for Ride Height Control of Automotive Semi-Active Air Suspension Systems. *IEEE Access* **2018**, *6*, 63777–63793. [CrossRef]
13. Nieto, A.; Morales, A.; Trapero, J.; Chicharro, J.; Pintado, P. An adaptive pneumatic suspension based on the estimation of the excitation frequency. *J. Sound Vib.* **2010**, *330*, 1891–1903. [CrossRef]
14. Eskandary, P.K.; Khajepour, A.; Wong, A.; Ansari, M. Analysis and optimization of air suspension system with independent height and stiffness tuning. *Int. J. Automot. Technol.* **2016**, *17*, 807–816. [CrossRef]
15. Ho, C.M.; Tran, D.T.; Ahn, K.K. Adaptive sliding mode control based nonlinear disturbance observer for active suspension with pneumatic spring. *J. Sound Vib.* **2021**, *509*, 116241. [CrossRef]
16. Zhao, R.; Xie, W.; Wong, P.K.; Cabecinhas, D.; Silvestre, C. Robust Ride Height Control for Active Air Suspension Systems with Multiple Unmodeled Dynamics and Parametric Uncertainties. *IEEE Access* **2019**, *7*, 59185–59199. [CrossRef]
17. Sun, X.; Yuan, C.; Cai, Y.; Wang, S.; Chen, L. Model predictive control of an air suspension system with damping multi-mode switching damper based on hybrid model. *Mech. Syst. Signal Process.* **2017**, *94*, 94–110. [CrossRef]
18. Sun, X.; Cai, Y.; Chen, L.; Liu, Y.; Wang, S. Vehicle height and posture control of the electronic air suspension system using the hybrid system approach. *Veh. Syst. Dyn.* **2016**, *54*, 328–352. [CrossRef]
19. Han, J. From PID to Active Disturbance Rejection Control. *IEEE Trans. Ind. Electron.* **2009**, *56*, 900–906. [CrossRef]
20. Li, S.; Yang, J.; Chen, W.-H.; Chen, X. Generalized Extended State Observer Based Control for Systems with Mismatched Uncertainties. *IEEE Trans. Ind. Electron.* **2011**, *59*, 4792–4802. [CrossRef]
21. He, W.; Tang, X.; Wang, T.; Liu, Z. Trajectory Tracking Control for a Three-Dimensional Flexible Wing. *IEEE Trans. Control. Syst. Technol.* **2022**, *30*, 2243–2250. [CrossRef]
22. Talole, S.E.; Kolhe, J.P.; Phadke, S.B. Extended-State-Observer-Based Control of Flexible-Joint System with Experimental Validation. *IEEE Trans. Ind. Electron.* **2009**, *57*, 1411–1419. [CrossRef]
23. Yao, J.; Jiao, Z.; Ma, D. Extended-State-Observer-Based Output Feedback Nonlinear Robust Control of Hydraulic Systems with Backstepping. *IEEE Trans. Ind. Electron.* **2014**, *61*, 6285–6293. [CrossRef]
24. Zhao, L.; Zhang, B.; Yang, H.; Wang, Y. Observer-Based Integral Sliding Mode Tracking Control for a Pneumatic Cylinder With Varying Loads. *IEEE Trans. Syst. Man Cybern. Syst.* **2018**, *50*, 2650–2658. [CrossRef]
25. Lau, J.Y.; Liang, W.; Tan, K.K. Motion Control for Piezoelectric-Actuator-Based Surgical Device Using Neural Network and Extended State Observer. *IEEE Trans. Ind. Electron.* **2019**, *67*, 402–412. [CrossRef]
26. Guo, Q.; Zhang, Y.; Celler, B.G.; Su, S.W. Backstepping Control of Electro-Hydraulic System Based on Extended-State-Observer With Plant Dynamics Largely Unknown. *IEEE Trans. Ind. Electron.* **2016**, *63*, 6909–6920. [CrossRef]
27. Chen, W.-H.; Yang, J.; Guo, L.; Li, S. Disturbance-Observer-Based Control and Related Methods—An Overview. *IEEE Trans. Ind. Electron.* **2015**, *63*, 1083–1095. [CrossRef]
28. Ba, D.X.; Dinh, T.Q.; Ahn, K.K. An Integrated Intelligent Nonlinear Control Method for a Pneumatic Artificial Muscle. *IEEE/ASME Trans. Mechatronics* **2016**, *21*, 1835–1845. [CrossRef]
29. Hamza, A.; Ben Yahia, N. Heavy trucks with intelligent control of active suspension based on artificial neural networks. *Proc. Inst. Mech. Eng. Part I J. Syst. Control. Eng.* **2020**, *235*, 952–969. [CrossRef]
30. Ahn, K.K.; Anh, H.P.H. Design and implementation of an adaptive recurrent neural networks (ARNN) controller of the pneumatic artificial muscle (PAM) manipulator. *Mechatronics* **2009**, *19*, 816–828. [CrossRef]
31. Hamza, A.; Ben Yahia, N. Intelligent Neural Network Control for Active Heavy Truck Suspension. In *Advances in Mechanical Engineering and Mechanics*; Springer Science and Business Media LLC: Cham, Switzerland, 2019; pp. 16–23.
32. Bao, W.N.; Chen, L.P.; Zhang, Y.Q.; Zhao, Y.S. Fuzzy adaptive sliding mode controller for an air spring active suspension. *Int. J. Automot. Technol.* **2012**, *13*, 1057–1065. [CrossRef]
33. Zhao, J.; Wong, P.K.; Xie, Z.; Wei, C.; He, F. Integrated variable speed-fuzzy PWM control for ride height adjustment of active air suspension systems. In Proceedings of the 2015 American Control Conference (ACC), Chicago, IL, USA, 1–3 July 2015; pp. 5700–5705.
34. Na, J.; Chen, Q.; Ren, X.; Guo, Y. Adaptive Prescribed Performance Motion Control of Servo Mechanisms with Friction Compensation. *IEEE Trans. Ind. Electron.* **2013**, *61*, 486–494. [CrossRef]
35. Bechlioulis, C.P.; Rovithakis, G.A. Robust Adaptive Control of Feedback Linearizable MIMO Nonlinear Systems With Prescribed Performance. *IEEE Trans. Autom. Control* **2008**, *53*, 2090–2099. [CrossRef]
36. Kong, L.; He, W.; Liu, Z.; Yu, X.; Silvestre, C. Adaptive Tracking Control with Global Performance for Output-Constrained MIMO Nonlinear Systems. *IEEE Trans. Autom. Control* **2022**, 1–8. [CrossRef]
37. Kong, L.; He, W.; Yang, W.; Li, Q.; Kaynak, O. Fuzzy Approximation-Based Finite-Time Control for a Robot with Actuator Saturation Under Time-Varying Constraints of Work Space. *IEEE Trans. Cybern.* **2020**, *51*, 4873–4884. [CrossRef]
38. CHo, C.M.; Nguyen, C.H.; Ahn, K.K. Adaptive Fuzzy Observer Control for Half-Car Active Suspension Systems with Prescribed Performance and Actuator Fault. *Electronics* **2022**, *11*, 1733.

39. Liu, Y.-J.; Chen, H. Adaptive Sliding Mode Control for Uncertain Active Suspension Systems with Prescribed Performance. *IEEE Trans. Syst. Man Cybern. Syst.* **2020**, *51*, 6414–6422. [CrossRef]
40. Wang, S.; Yu, H.; Yu, J.; Na, J.; Ren, X. Neural-Network-Based Adaptive Funnel Control for Servo Mechanisms With Unknown Dead-Zone. *IEEE Trans. Cybern.* **2018**, *50*, 1383–1394. [CrossRef] [PubMed]
41. Na, J.; Huang, Y.; Wu, X.; Gao, G.; Herrmann, G.; Jiang, J.Z. Active Adaptive Estimation and Control for Vehicle Suspensions with Prescribed Performance. *IEEE Trans. Control Syst. Technol.* **2018**, *26*, 2063–2077. [CrossRef]
42. Liu, Y.-J.; Zeng, Q.; Tong, S.; Chen, C.L.P.; Liu, L. Actuator Failure Compensation-Based Adaptive Control of Active Suspension Systems with Prescribed Performance. *IEEE Trans. Ind. Electron.* **2019**, *67*, 7044–7053. [CrossRef]
43. Kostarigka, A.K.; Rovithakis, G.A. Adaptive dynamic output feedback neural network control of uncertain MIMO nonlinear systems with prescribed performance. *IEEE Trans. Neural Netw. Learn. Syst.* **2012**, *23*, 138–149. [CrossRef]
44. Liu, H.; Li, X.; Liu, X.; Wang, H. Adaptive Neural Network Prescribed Performance Bounded-Hinfinity Tracking Control for a Class of Stochastic Nonlinear Systems. *IEEE Trans. Neural Netw. Learn. Syst.* **2020**, *31*, 2140–2152. [CrossRef] [PubMed]
45. Kim, C.; I Ro, P. A sliding mode controller for vehicle active suspension systems with non-linearities. *Proc. Inst. Mech. Eng. Part D J. Automob. Eng.* **1998**, *212*, 79–92. [CrossRef]
46. De Melo, F.J.M.Q.; Pereira, A.B.; Morais, A.B. The Simulation of an Automotive Air Spring Suspension Using a Pseudo-Dynamic Procedure. *Appl. Sci.* **2018**, *8*, 1049. [CrossRef]
47. Yang, Y.; Tan, J.; Yue, D. Prescribed performance control of one-DOF link manipulator with uncertainties and input saturation constraint. *IEEE/CAA J. Autom. Sin.* **2019**, *6*, 148–157. [CrossRef]
48. Pu, Z.; Yuan, R.; Yi, J.; Tan, X. A Class of Adaptive Extended State Observers for Nonlinear Disturbed Systems. *IEEE Trans. Ind. Electron.* **2015**, *62*, 5858–5869. [CrossRef]
49. Zheng, L.Q.G.Q.; Gao, Z. On stability analysis of active disturbance rejection control for nonlinear time varying plants with unknown dynamics. In Proceedings of the IEEE Conference on Decision and Control, New Orleans, LA, USA, 12–14 December 2007; pp. 3501–3506.
50. Ge, S.; Wang, C. Adaptive Neural Control of Uncertain MIMO Nonlinear Systems. *IEEE Trans. Neural Netw.* **2004**, *15*, 674–692. [CrossRef]
51. Liu, Y.-J.; Li, J.; Tong, S.; Chen, C.L.P. Neural Network Control-Based Adaptive Learning Design for Nonlinear Systems with Full-State Constraints. *IEEE Trans. Neural Netw. Learn. Syst.* **2016**, *27*, 1562–1571. [CrossRef] [PubMed]
52. Zuo, L.; Nayfeh, S. Low order continuous-time filters for approximation of the ISO 2631-1 human vibration sensitivity weightings. *J. Sound Vib.* **2003**, *265*, 459–465. [CrossRef]

Disclaimer/Publisher's Note: The statements, opinions and data contained in all publications are solely those of the individual author(s) and contributor(s) and not of MDPI and/or the editor(s). MDPI and/or the editor(s) disclaim responsibility for any injury to people or property resulting from any ideas, methods, instructions or products referred to in the content.